Chapter 5

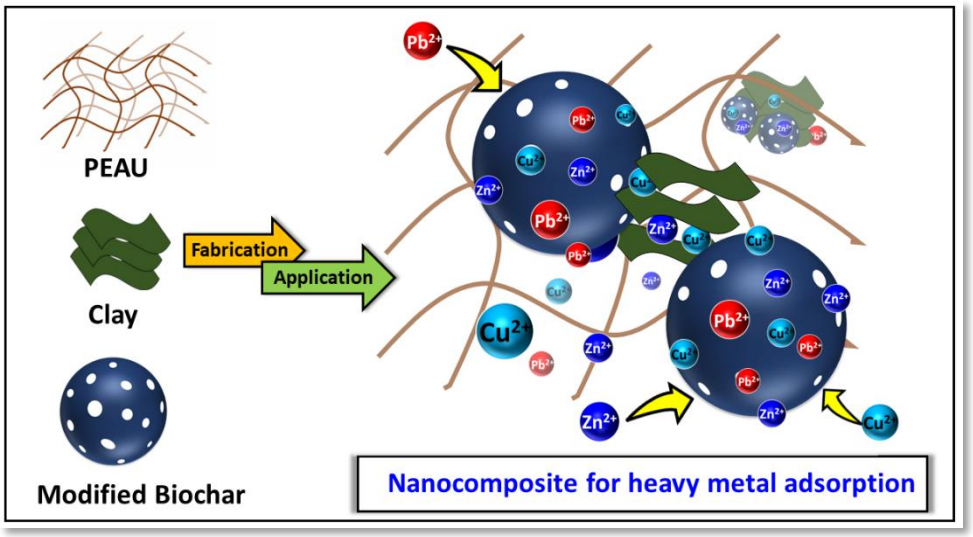
PEAU
Clay
Modified Biochar
Fabrication
Application
Nanocomposite for heavy metal adsorption

Poly(ester amide urethane) nanocomposites with biochar and bentonite clay for environmental remediation

Highlights

The trend towards incorporating environmentally friendly reinforcing agents in polymer nanocomposites has led to increased exploration of various naturally derived biomass products. Over the years, biochar, in particular has gained attention for its potential to replace traditional reinforcing agents which are mostly inorganic in nature. In this study, we detail the fabrication of biochar from kraft lignin, followed by its modification with epichlorohydrin and triethylamine, and its integration into a poly(ester amide urethane) matrix along with bentonite nanoclay particles to produce a polymer nanocomposite via a feasible approach. The structural assessment was conducted using various instrumental techniques, including FTIR, PXRD, XPS, etc. In turn, the polymer nanocomposite exhibited enhanced mechanical features, with an impressive toughness value of 87.45 MJ/m^3 along with a 160% increment in tensile strength compared to the pristine poly(ester amide urethane) matrix. Additionally, the polymer nanocomposite showed significant improvements in thermal properties with T_g values rising acutely from -28.15 to 84.56 °C, while also demonstrating sustainability through inherent biodegradability attributes. Beyond their structural strength and thermal stability, the polymer nanocomposite showed great promise as adsorbents, effectively removing heavy metal ions, viz., Pb(II), Zn(II), and Cu(II) ions from aqueous systems with removal efficiencies of 80.38%, 76.06%, and 70.80%, respectively. A detailed kinetics study identified the pseudo-second order (PSO) model as the most accurate tool for assessing the heavy metal ions removal process. Furthermore, the Langmuir adsorption isotherm provided insights into the sorption characteristics of the polymer nanocomposite. Overall, the polymer nanocomposite exhibited impressive recovery capability over five cycles, highlighting their economic feasibility as well as sustainability.

Parts of this chapter are ready to be communicated as

Kar, A., and Karak, N. Tailored biochar infused poly(ester amide urethane) nanocomposite for efficient heavy metal ion removal.

5.1. Introduction

In response to the burgeoning demand for various smart materials, different conventional substances, viz., glass, ceramics as well as metals have been supplanted by various polymer composites, primarily owing to their attributes of facile processing techniques, lightweight composition, and economical production as explained in **Chapter 4**. Across the years, polymer composites have found extensive applications in different genres, ranging from high-end industrial items to economical household products. In turn, the plastic industry has experienced significant growth, attributed to its diverse applications across various sectors [1]. This surge is ascribable to the amplified requirements from manifold industrial sectors encompassing versatile domains, viz., packaging, automotive, aerospace, construction, etc. The versatility of polymers, characterized by their commendable strength, cost-effectiveness, lightweight nature, corrosion resistance, etc. has played a pivotal role as an important factor for driving this robust growth as enumerated in **Chapter 3**.

Despite the manifold merits associated with polymers, inherent shortcomings in their components, viz., inadequate flame retardancy, diminished thermal stability, suboptimal conductivity, etc. persist [2, 3]. In order to surmount these challenges, considerable research efforts have been directed towards augmenting and tailoring the polymer composites properties, especially by conducting addition of fillers, which emerged as an effective strategy [4]. A plethora of investigations carried out by researchers across the globe have delved into these issues, seeking pragmatic solutions. In light of the escalating preferences for sustainable, cost-effective, and environmentally friendly materials, biochar has garnered significant attention as a reinforcing agent as clarified extensively in **Chapter 4**. This interest arises as a compelling alternative to conventional carbon fillers namely graphene, carbon black as well as carbon nanotubes, which are mostly beset by economic viability and environmental concerns. Unlike other carbon fillers that require complex methods of production, biochar, a carbonaceous porous solid matter, can be generated by gradual pyrolyzing of biomass at higher temperatures, viz., 500-800 °C [5, 6]. Similar to its carbon counterparts, biochar is characterized by thermal stability, large surface area, porosity and encompasses different functional groups, namely carboxyl, hydroxyl, and carbonyl. The utilization of biomass for biochar production as a filler in polymer composites not only addresses the waste management issues but also underscores the

potential of biomass for generating high-value added products as elucidated elaborately in **Chapter 4**.

Over the course of these years, modification of biochar material has been regarded as a strategic approach in order to optimize its performance, tailor its intrinsic properties as well as increase its suitability for specific environmental remediation challenges. Many reports stated that the modification of the biochar material resulted in surface area enhancement, introduction of specific functional groups along with charge adjustment and hydrophobicity traits. One of the most common approaches of modification of biochar material is chemical functionalization, where reactive chemicals are invoked to incorporate specific functional groups to the periphery of the biochar material. In turn, surface modification involves treating the biochar material with various oxidizing agents in order to augment its reactivity [7]. Steam activation also aids in enhancing the surface area and porosity of biochar material for various applications. Impregnation, another modification method, entails introducing substances, viz., metal nanoparticles to improvise the adsorption or catalytic capabilities. Furthermore, pyrolysis conditions can be adjusted to influence the biochar's chemical as well as physical characteristics. Doping with various additives, viz., nitrogen substances, also helps in modifying the electronic features and the biological treatment involving different microbes, aid in enhancing the nutrient retention for different soil amendments [8, 9]. Therefore, the choice of method depends on the desired applications, as each method provides unique advantages for tailoring the biochar material to various specific utilities. For example- Li et al. in 2022 carried out post treatment on biochar obtained from bamboo, by treating it with sulfur, which aided in increasing the soil pH and the amount of organic residues followed by creating immobilization of Cd element [10]. Similarly, Wang et al. in 2020 conducted post treatment on the biochar material by using KOH, which resulted in increment in the pore volume and surface area, facilitating immobilization of Pb element [11]. Many other studies reported on the introduction of goethite into the biochar material obtained from pyrolysis of wheat straw, which resulted in creating more functional groups, viz., Fe-O as well as increment in surface area, thereby allowing facile reduction of phosphate and arsenic [12].

In contemporary times, the accelerated pace of industrialization and urbanization has led to substantial discharge of sewage and industrial effluents containing elevated levels of heavy metals into both underground and surface water bodies. This poses a persistent and concerning global environmental issue due to the non-biodegradable, inherent toxicity, and the potential bioenrichment risk in the food chain associated with these inorganic pollutants. Consequently, finding an efficacious treatment for heavy metals has become imperative. Amongst the heavy metals stemming from anthropogenic activities, lead (Pb), copper (Cu), and zinc (Zn) are particularly recognized for their harmful repercussions on human health and their widespread prevalence as contaminants in soils and aqueous environments [13]. In the realm of water treatment technologies dedicated to heavy metal removal, adsorption stands out as a prominent approach on the ground of its high efficiency and simple mode of operation. Despite the prevalence of various adsorbents developed over the past decades, such as iron oxides, zeolites, and other carbon-based materials, with strong affinity for heavy metals in aqueous solutions, their widespread practical application is hindered by being prohibitively costly and time-consuming [14]. Consequently, substantial efforts have been directed towards the development of novel adsorbents characterized by high adsorption capacity. In this milieu, biochar plays a pivotal role as a promising adsorbent on ground of its expansive surface area, ease of recycling, diverse functional groups, and other advantageous characteristics. Despite biochar's inherent advantages, including surface groups and abundant sources, its unaltered form falls short in achieving optimal pollutant removal efficiency. Consequently, research efforts have significantly shifted towards the development of biochar-based composites and nanohybrids [13]. For example- Xiang et al. fabricated a composite material by impregnating biochar material with MgO particles for carrying out cadmium adsorption. It was noted that the adsorption capacity of the modified biochar markedly surpassed the unaltered form by three times factor [15]. Similarly, Zhou et al. in a separate study investigated the adsorption of copper ions using a biochar/MnO_2 nanohybrid derived from corn stalks. The comparative analysis revealed higher adsorption capacity of nanohybrid which underscores the substantial impact of loading of nano MnO_2 particles onto the biochar surface [16]. Furthermore, biochar derived from orange peel powder demonstrated effective utilization for the removal of cadmium ions from industry wastewater through the incorporation of iron oxide nanoparticles.

Therefore, in our study, we made an attempt to conduct the synthesis of a nanohybrid, fabricated by integrating bentonite nanoclay as well as modified biochar particles. Subsequently, the modification of the biochar material derived from kraft lignin was carried out using epichlorohydrin and triethylamine. Both the modified biochar material and the nanoclay particles served as reinforcing agents into the polymer matrix. The latter was synthesized by invoking an environmentally benign route via a melt polycondensation method. The nanomaterial and the nanocomposite were further evaluated using various instrumental analyses and different tests were performed on them. These evaluations were conducted to imbue certain distinct properties considered beneficial for applications in different fields, with particular emphasis on heavy metal ions removal systems.

5.2. Experimental

5.2.1. Materials

A range of chemicals, including citric acid anhydrous, glycerol anhydrous, hexamethylene diamine, PVA, KOH, oxalic acid, NaOH, and p-TSA were employed. The specifications for these chemicals align with the detailed discussions provided in **Chapter 2**. Additionally, IPDI and DMSO were utilized, and their complete specifications are outlined in **Chapter 3**. Kraft lignin and phosphoric acid were used, and the detailed specifications are provided in **Chapter 4**. In the context of biodegradation study, the bacterial strain, viz., *Bacillus subtilis* was employed, as specified in **Chapter 2**.

Epichlorohydrin was procured from SRL, India and utilized in its original form without any additional modifications. It is a clear liquid with a pungent odor, bearing a density of 1.18 g/cm^3 and molecular weight of 92.52 g/mol.

Triethylamine, a colorless liquid, with an ammonia like odor, was acquired from Avantor, India. It bears a density value of 0.726 g/cm^3 and molecular weight of 101.19 g/mol.

Lead (II) nitrate, characterized as a white inorganic compound with a density value of 4.53 g/cm^3 and molecular weight of 331.2 g/mol, was obtained from Merck, India and directly utilized in its original form for the investigation of adsorption of metal ions.

Copper (II) chloride dihydrate, a blue-green colored copper complex bearing a molecular

weight of 170.48 g/mol was procured from Merck, India. It was used as received for conducting the study of adsorption of metal ions.

Zinc (II) nitrate hexahydrate, characterized as a white, crystalline compound with a density value of 2.06 g/cm^3 and molecular weight of 297.49 g/mol, was procured from Merck, India and utilized as received for carrying out the investigation of adsorption of metal ions.

Bentonite nanoclay, a beige colored compound in its powder form was used in the fabrication of polymer nanocomposite. It bears a bulk density value lying within the range of 600-1100 kg/m^3 with an average size of the particles less than 25 micron.

5.2.2. Methods

5.2.2.1. Synthesis of modified biochar

As described in **Chapter 4**, biochar was synthesized from kraft lignin via a controlled pyrolysis process. The kraft lignin was subjected to pyrolysis, a thermal degradation process at 450 °C for 1.5 h which resulted in the formation of the biochar, a carbon-rich material characterized by its porous structure and varied surface functionalities. Following the synthesis, the modification of biochar was carried out chemically which entailed the use of epichlorohydrin and triethylamine. 0.5 g of biochar was introduced into a glass vial and was stirred continuously with a gradual increment in the temprature up to 60 °C. Subsequently, this was followed by slow dropwise addition of 3N NaOH solution along with an equal amount of epichlorohydrin and triethylamine (1 mL each) into the reaction vessel. The reaction mixture was allowed to proceed continuously for a time duration of 2 h and was monitored closely until an observable increase in viscosity occurred. In the succeeding steps, the reaction contents along with 5 mL of THF solvent was transferred into centrifugation tubes and centrifugation was carried out at 5000 rpm for 20 minutes. This step was repeated thrice and was primarily executed to purify the modified biochar particles. These modified biochar particles were further employed as reinforcing agents in the fabrication of the polymer nanocomposite.

5.2.2.2. Preparation of modified biochar/ bentonite clay/ poly(ester amide urethane) nanocomposite

The synthesis of polymer nanocomposite involved integrating the modified biochar

material and the bentonite nanoclay particles into the polymer matrix using an *in-situ* approach. As described in **Chapter 2**, the polymer base, viz., the poly(ester amide) resin was synthesized through melt polycondensation using glycerol, hexamethylene diamine, and citric acid as the primary substrates via a one-pot reaction. The reaction mixture underwent continuous heating at 140 °C for a time span of 3 h under vacuum conditions, resulting in the formation of a thick, viscous substance before reaching the gelation point. Subsequently, an effort was made to enhance the strength and texture of the polymeric films by introducing PVA into the polymer matrix using DMSO as the solvent. The reaction mixture was then consistently heated at 80 °C for 1 h until a uniform mixture was achieved. Following this, the modified biochar particles dispersed in 1 mL of DMSO solvent were added. Alternatively, 0.5 g of bentonite nanoclay particles were dispersed in minimum amount of water and was stirred continuously overnight. This was followed by addition of these dispersed bentonite nanoclay particles into the reaction mixture along with the modified biochar particles. Subsequently, the reaction proceeded for an additional 1 h, after which IPDI was added in a dropwise manner as described in the previous chapter [17]. Furthermore, the entire process continued for an additional 45 minutes at 60 °C until complete consumption of isocyanate occurred under the specified reaction parameters. The comprehensive fabrication process of polymer nanocomposite is elucidated in **Scheme 5.1**. Upon completion of the reaction, the polymeric constituents underwent sonication in an ultra-bath sonicator for a time duration of 30 minutes. This step was crucial to agitate the modified biochar as well as the bentonite nanoclay particles and ensure a homogeneous dispersion throughout the reaction mixture. Subsequently, the contents of the reaction mixture were transferred onto Teflon sheets and subjected to drying at 55 °C in a conventional drying oven for a time period of two to four days. This initial drying phase was followed by a subsequent drying step at an elevated temperature, specifically 70-75 °C, for a time span of five to seven days until the polymeric films reached a touch-free state. Throughout this entire process, meticulous care was taken to facilitate uniform dispersion of modified biochar and nanoclay particles as well as to achieve optimal conditions for conducting subsequent analyses. After the completion of the drying steps, the polymeric films were carefully extracted from the hot-air oven and utilized for different analytical procedures. The fabricated nanocomposite was assigned as PEAU-MBC/clay. In a similar way, the modified biochar/ poly(ester amide urethane) nanocomposite designated as PEAU/MBC was prepared by incorporating the modified biochar particles

into the polymer matrix as mentioned above. In a corresponding manner, bentonite nanoclay/ poly(ester amide urethane) nanocomposite was fabricated by integrating the bentonite nanoclay particles into the polymer matrix following thorough stirring of the bentonite clay nanoparticles/ water dispersion overnight as detailed extensively above and designated as PEAU/clay.

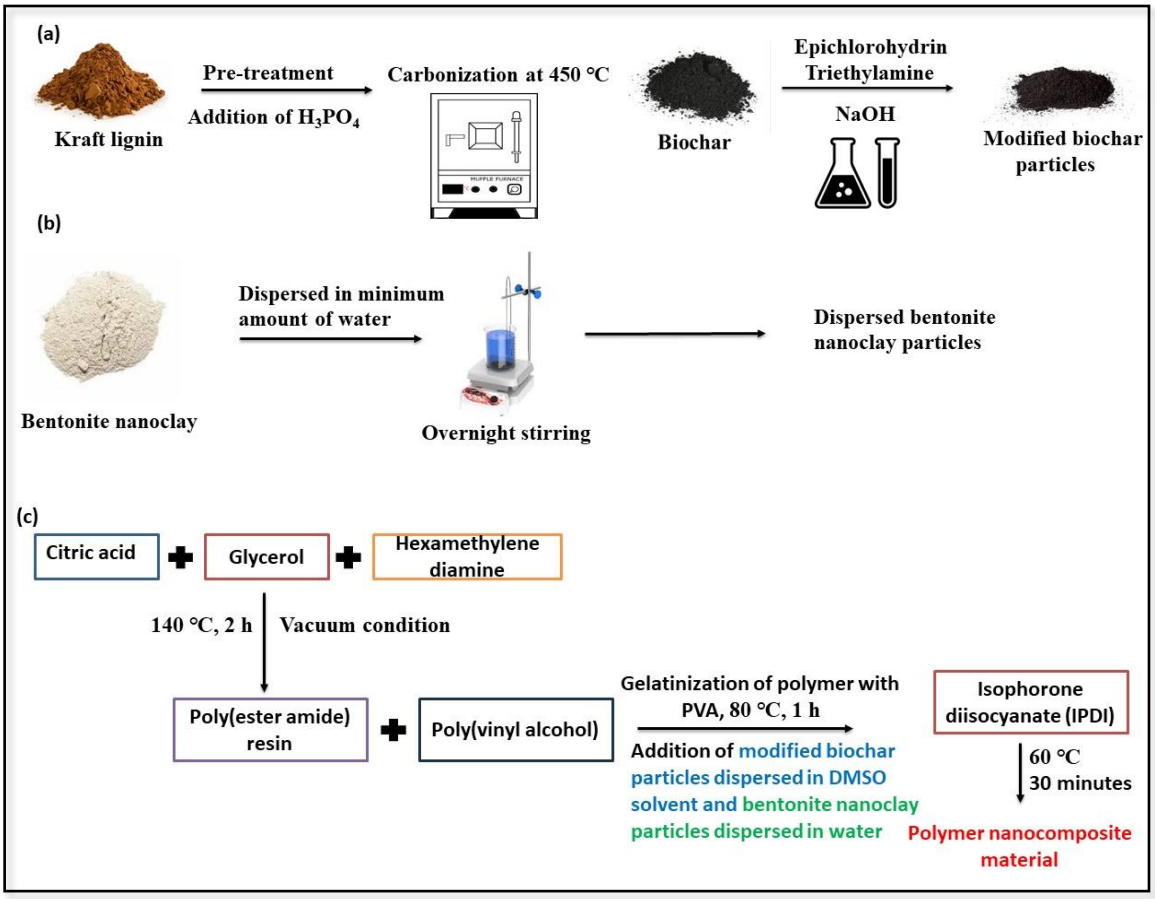

Scheme 5.1. Scheme for **(a)** synthesis of modified biochar particles, **(b)** preparation of dispersed bentonite nanoclay particles, and **(c)** fabrication of polymer nanocomposite integrated with modified biochar and bentonite nanoclay particles.

Both the poly(ester amide urethane) nanocomposites were fabricated at various weight percentages of modified biochar as well as bentonite nanoclay particles as outlined in **Table 5.1.**

5.2.3. Characterization

5.2.3.1. Structural analysis

The synthesized modified biochar material, poly(ester amide urethane) nanocomposites incorporating modified biochar and bentonite nanoclay loadings as well as the modified biochar/ bentonite clay/ poly(ester amide urethane) nanocomposite underwent comprehensive characterization using a variety of analytical and spectroscopic techniques.

Table 5.1. Different compositions of poly(ester amide) resin, IPDI, PVA, modified biochar and bentonite clay nanoparticles.

Sample code	PEA (g)	PVA (g)	IPDI (g)	Modified biochar (wt%)	Bentonite nanoclay (wt%)
PEAU-MBC/clay	1	0.6	0.2	0.5	0.5
PEAU/MBC	1	0.6	0.2	0.5	-
PEAU/clay	1	0.6	0.2	-	0.5

These methods comprised of FTIR spectroscopy, PXRD, XPS study, BET analysis, proximate and ultimate analysis, SEM-EDX and FESEM study. In **Chapter 2**, a detailed discussion on the instrumentation for FTIR spectroscopy has already been provided. Similarly, **Chapter 3** explicitly enumerates the specific instrumentation details for both XPS and PXRD analyses. In turn, **Chapter 4** broadly outlines the instrumentation details for elemental as well as BET analysis. It also entails the minute details of instrumentation for proximate analysis, SEM-EDX as well as FESEM analyses. Moreover, **Chapter 2** and **Chapter 3** meticulously discusses all other instrumentation and methodologies used to evaluate the performance characteristics, including thermal, mechanical, and biodegradation (bacterial degradation and soil burial study) properties.

5.2.3.2. Metal ion adsorption study

The preparation of stock solutions involved dissolving accurately weighted $CuCl_2.2H_2O$, $Pb(NO_3)_2$, and $Zn(NO_3)_2.6H_2O$ in distilled water, resulting in concentrations of 1000 ppm. The experimental solutions were then prepared via further dilutions using double deionized water bearing a conductivity value of 18.2 μScm^{-1}. Additionally, in the batch equilibrium adsorption tests, 50 mL of Pb(II), Cu(II) and Zn(II) solutions were employed.

In turn, following the sorption process, the separation of the sorbent molecules from the samples were achieved through filtration procedures, and subsequent analysis of the filtrate solutions was conducted using the atomic absorption spectrophotometer bearing the model number UK: AAS/ICE 3500.

The polymeric films of the modified biochar/ bentonite clay/ poly(ester amide urethane) nanocomposite were cut into small pieces and immersed in solutions containing Cu^{2+}, Pb^{2+}, and Zn^{2+} ions at varying concentrations under stirring conditions. Subsequently, the metal-ion containing solutions were extracted at fixed time intervals post the adsorption process. An atomic absorption spectrophotometer as described above was employed to ascertain the residual metal ion concentrations, which were then utilized to assess the removal efficiency as well as the adsorption capacity of metal ions using **Equations 4.1.** and **4.2.** as described extensively in the previous chapter. In turn, to examine the adsorption performance of the PEAU-MBC/clay nanocomposite under varied conditions, different variables, viz., temperature, pH, adsorbent dosage, adsorption time, and metal ion concentrations were systematically altered. The adsorbent dosages for metal ions were eventually adjusted based on the adsorbent's capacity for each particular metal ion. Additionally, the pH of the metal ion solutions varied from pH values ranging from 2 to 10. Moreover, the adsorption capacity parameter was investigated at different metal ion concentrations ranging from 20 ppm to 200 ppm as well as at temperature values, viz., room temperature, 313 K, and 323 K. The adsorption times attained at equilibrium for each metal ion were determined separately by assessing the remaining metal ion concentrations at various time intervals using an atomic absorption spectrophotometer [18].

Moreover, to assess the recyclability of the PEAU-MBC/clay nanocomposite, following the achievement of equilibrium adsorption, the adsorbent, i.e., the polymeric films of the PEAU-MBC/clay nanocomposite underwent washing with 0.1 N HCl solution for further utilization in subsequent cycles of adsorption phenomenon. Subsequently, the removal efficiency was once again ascertained using the atomic absorption spectrophotometer methodology [19].

5.3. Results and discussion

5.3.1. Synthesis of modified biochar

As described in the previous chapter, biochar preparation involved carbonizing the kraft ;ignin powder at elevated temperatures, thereby initiating decomposition by breaking the weaker bonds, including the hydrogen as well as C-OH bonds. With the eventual rise in temperature, various robust bonds such as β-O-4 linkages were subsequently cleaved. In the low-temperature zone, different compounds, viz., guaicyl hydroxyl entities and styrene are formed, thereby progressing to cresols and catechol in the higher temperature phases. Consequently, the rupture of β-O-4 linkages resulted in generation of free radicals which further facilitated the lignin depolymerization. Moreover, at temperatures above 300 °C, random repolymerization phenomenon led to the biochar formation. Under this context, modification of the biochar material obtained from kraft lignin was carried out chemically which aimed at improving the functional properties and entailed the use of epichlorohydrin and triethylamine. In this method, biochar was subjected to the reactivity of epichlorohydrin, a bifunctional epoxy compound, in the presence of NaOH and triethylamine, which acted as a crosslinking agent. On introduction of epichlorohydrin to the system containing various hydroxyl groups on the periphery of the biochar material, it underwent nucleophilic substitution reaction which resulted in attachment of epoxide groups on the surface of biochar [20]. Additionally, triethylamine, which acted as a crosslinking agent, reacted with the epoxide group on the biochar, leading to the formation of a crosslinked structure. Moreover, the nucleophilic attack of triethylamine on the epoxide groups resulted in the formation of stable linkages, thereby facilitating the incorporation of new functional groups on the biochar surface as shown in **Scheme 5.2.** This aided in imparting tailored chemical characteristics. It also aimed at enhancing biochar's adsorption capabilities, reactivity, and overall versatility for different applications. The controlled introduction of the functional moieties through this chemical pathway added a new level of customization to biochar material, thereby allowing researchers to finely tune its properties based on specific application requirements [19].

5.3.2. Fabrication of modified biochar/ bentonite clay/ poly(ester amide urethane) nanocomposite

The modified biochar/ bentonite clay/ poly(ester amide urethane) nanocomposite was synthesized through a one pot *in-situ* method, utilizing modified biochar and bentonite nanoclay particles as the reinforcing materials. The initial fabrication of the core poly(ester amide) resin involved a polycondensation method among the prime substrates, viz., citric

acid, glycerol, and hexamethylene diamine, as elucidated in **Chapter 2**. The adoption of a one-pot synthesis technique prioritized minimal chemical usage, streamlined procedures for scalable industrial production, and efficient time management. Provided the brittle consistency of poly(ester amide) resin, IPDI and PVA were introduced to bolster the polymeric matrix through polyaddition reactions between the hydroxyl and isocyanate functional groups. Furthermore, the introduction of urethane linkages into the parent

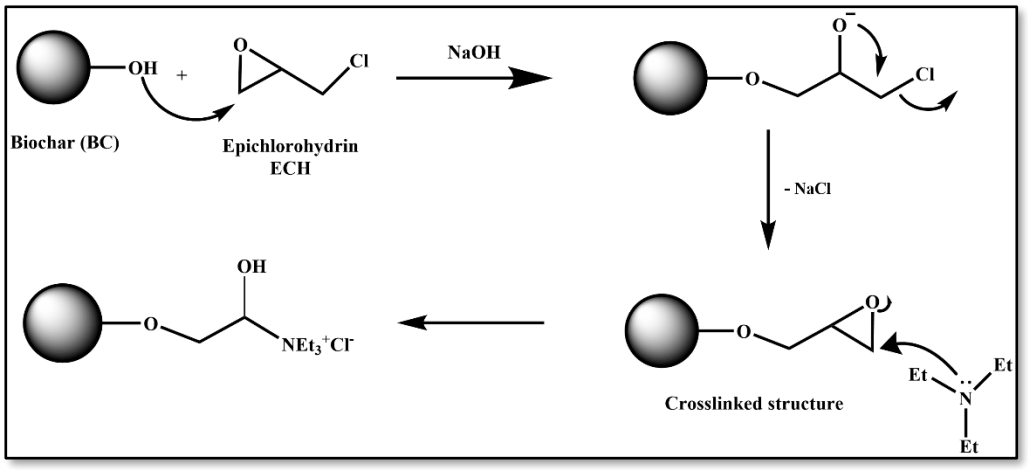

Scheme 5.2. Fabrication of modified biochar particles using epichlorohydrin and triethylamine

polymeric resin resulted in the fabrication of poly(ester amide urethane) resin, as extensively discussed in **Chapter 3**. Subsequently, the modified biochar particles were added to the polymer matrix dispersed in a minimal amount of DMSO solvent. This was followed by addition of bentonite nanoclay particles dispersed in minimum amount of water. The entire reaction sequence, inclusive of all the steps, occurred through continuous mechanical stirring to facilitate the homogeneous blending of reactants, modified biochar particles as well as bentonite nanoclay particles. As a result, the polar functional groups present in the poly(ester amide urethane) resin interacted with the polar groups of modified biochar as well as bentonite nanoclay particles, thereby contributing to the overall stability of the nanohybrid unit. The homogeneous distribution of the modified biochar particles along with the bentonite nanoclay particles within the polymer matrix ensured refinement of different performance features. Dipole-dipole, van der Waals, hydrogen bonding and electrostatic forces of interactions played crucial roles in fostering connections amongst the polymer matrix, modified biochar and bentonite nanoclay particles. The oxygen

present in the functional groups of biochar, viz., carbonyl or hydroxyl groups, engaged in hydrogen bonding interactions with the hydrogen present in the hydroxyl containing sites on the bentonite nanoclay particles as well as with the hydroxyl or urethane moieties existing within the poly(ester amide urethane) matrix. This aided in enhancing the adhesion among the polymer matrix, modified biochar and bentonite nanoclay particles. Additionally, the polar functional groups present in the biochar material, i.e. the carbonyl and hydroxyl groups, engaged with the polar regions of the bentonite nanoclay particles as well as the poly(ester amide urethane) matrix through dipole-dipole interactions, resulting in the creation of attractive forces of interactions [20]. Correspondingly, bentonite nanoclay particles, being layered silicates, exhibit a net negative charge on their surface on ground of isomorphic substitution of ions in the crystal lattice. Biochar particles also possess charged functional groups. Under this pretext, electrostatic interactions between the charged sites on the particles played an important role in influencing their dispersion and aggregation potential [21]. Overall, these interactions played an important role in influencing the intermolecular forces among the polymer matrix, modified biochar and bentonite nanoclay particles, thereby shaping the properties of the polymer nanocomposite.

5.3.3. Characterization of modified biochar obtained from kraft lignin and modified biochar/ bentonite clay/ poly(ester amide urethane) nanocomposite

5.3.3.1. Proximate and ultimate analysis

The proximate analysis of the modified biochar material aimed to assess its fundamental chemical composition, encompassing variables such as moisture content, fixed carbon, ash and volatile matter. **Table 5.2.** provided a comprehensive overview of these parameters. As per the previous findings reported in **Chapter 4**, an elevation in pyrolysis temperature correlated with reduction in the volatile matter due to the complete carbonization process. This increase in the carbonization temperature led to an ultimate rise in the ash content, accompanied by reduction in the fixed carbon matter. In our study, it was found that after modification of the biochar, there was a slight drop in the ash content from 3.06 to 2.47% along with a trivial increment in the volatile matter from 5.12 to 5.20%. Subsequently, no such prominent change was observed in the fixed carbon content in modified biochar in

comparison to its unmodified counterpart. The outcomes are in complete agreement with the findings reported by Peiris et al. and Zhao et al. [22, 23]

Table 5.2. Proximate analysis of modified biochar obtained from kraft lignin.

Volatile matter (wt%)	Ash (wt%)	Moisture content (wt%)	Fixed C (wt%)
5.20±0.78	2.47±0.07	6.71±0.57	85.62±0.27

The comprehensive examination of modified biochar material involved evaluating its elemental composition, encompassing varying proportions of oxygen, carbon, phosphorus, sulfur, and other elements. The results obtained offer valuable inputs into the chemical composition of the modified biochar material. **Table 5.3.** illustrated the findings of the ultimate analysis procedure conducted on the modified biochar derived from kraft lignin. The modified biochar material exhibited a greater carbon content comprising 75.13% of mass fraction, along with an oxygen content of 22.31%. It has been found that there was a slight increment in the oxygen content from 21.74% (unmodified biochar) to 22.31% on the ground of formation of new oxygen bearing functional groups. In turn, the increased carbon mass fraction is caused due to the formation of carbon entities which are condensed in nature due to extensive polymerization reactions. Consequently, the H/C ratio was observed to be exceptionally low at 0.034, indicating a high degree of carbonization as well as aromatization. Furthermore, the O/C ratio was observed to be notably low at 0.296. However, a slight rise in the ratio from 0.292 to 0.296 was recorded on the ground of introduction of new oxygen bearing functional moieties [19].

Table 5.3. Ultimate analysis of modified biochar obtained from kraft lignin.

C (wt%)	H (wt%)	O (wt%)	O/C	H/C
75.13	2.56	22.31	0.296	0.034

5.3.3.2. BET analysis

The evaluation of the specific surface area of diverse porous materials, such as biochar, employs the BET method. This approach furnishes valuable insights into different surface

properties of biochar material, facilitating its applications in various contexts. The specific surface area is determined to be 1244.17 m^2/g, accompanied by a pore size of 3.5 nm and a pore volume of 0.446 cm^3/g, as indicated by the desorption results obtained through the BJH (Barrett Joyner Halenda) method. As discussed in the previous chapter, a greater specific surface area value signifies biochar materials with greater porosity as well as increased reactivity values. In the present study, it was observed that there was a significant increment in the surface area of the biochar material upon modification from 1038.35 to 1244.17 m^2/g. This increase in surface area can be attributed to the introduction of oxygen bearing functional groups along with the elimination of certain walls existing within the carbonaceous materials. Additionally, the modified biochar material exhibited mesoporous characteristics as the pore sizes fell within the range of 2-50 nm as suggested by the pore size distribution studies. Furthermore, the N_2 adsorption-desorption isotherm, depicted in **Figure 5.1. (a)**, reflected the enhanced N_2 adsorption at lower partial pressure, underscoring the filling up of mesopores. Moreover, the presence of hysteresis between 0.50 and 0.65 relative pressure supported the assertion that the modified biochar material featured mesopores, as reported in different literature studies [17].

5.3.3.3. FTIR analysis

FTIR is perceived as a powerful analytical method to analyze and identify the functional groups present in the modified biochar material, polymer nanocomposites based on the absorption of infrared radiation. In the context of modification of biochar with epichlorohydrin and triethylamine, an FTIR analysis provided insights into the chemical composition as well as structural changes induced by the crosslinking process. **Figure 5.1. (b)** enumerated the FTIR spectra of both unmodified as well as modified biochar obtained from kraft lignin. As stated in the previous chapter, biochar displayed a broad and pronounced IR peak at 3420 cm^{-1} indicating -OH stretching vibrations and at 2936 cm^{-1}, signifying -CH stretching vibrations. In turn the presence of IR peaks in the 1700-1640 cm^{-1} range suggested the presence of carbonyl functional groups. Both the modified as well as unmodified biochar displayed identical IR absorption peaks, with the notable exception of a distinct sharp IR absorption peak at 1276 cm^{-1} observed in the modified biochar material, which is absent in the unmodified counterpart. This peak highlighted the existence of -C-O stretching vibrations in the biochar material introduced upon modification with epichlorohydrin and triethylamine. Additionally, the disappearance of

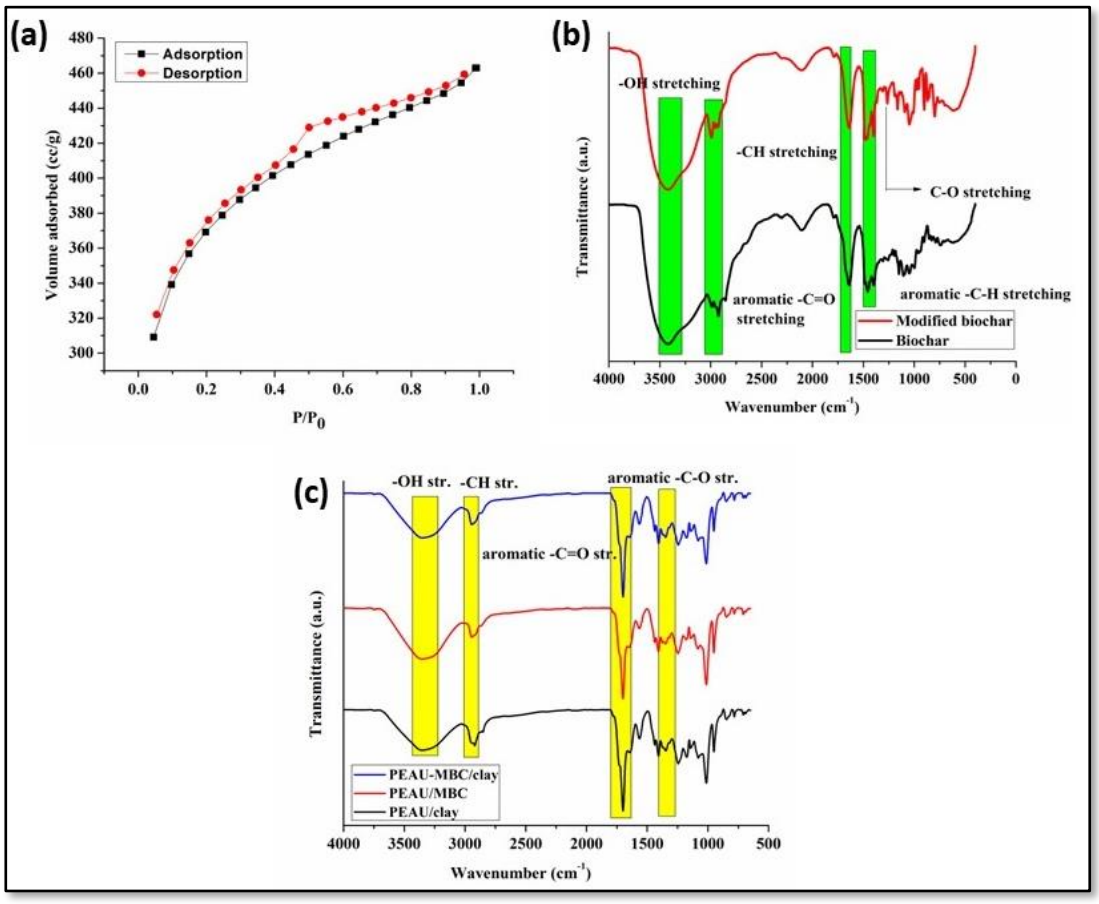

Figure 5.1. (a) BET adsorption-desorption curves of modified biochar material, **(b)** FTIR spectra of unmodified and modified biochar material, and **(c)** FTIR spectra of polymer nanocomposites.

characteristic peaks of -C-Cl (760 cm^{-1}) and epichlorohydrin, viz., epoxy (854 cm^{-1}) in the FTIR spectra of modified biochar material suggested the opening of the epoxy ring, which further reinforces the successful crosslinking of the biochar material through the formation of oxygen containing functional groups, viz., ether linkages [24]. FTIR analysis was also employed to identify the functional groups existing within the polymer nanocomposites and the results were subsequently compared with those of the parent polymer matrix. The analysis indicated that the polymer nanocomposite entailing modified biochar and bentonite nanoclay as the reinforcing agents, respectively exhibited characteristic IR absorption peaks similar to those observed in poly(ester amide urethane) resin, suggesting a comparable structure between the polymer matrix as well as the polymer nanocomposites. The chemical compositions of the PEAU-MBC/clay nanocomposite deviated from the parent polymer matrix on ground of inclusion of bentonite nanoclay and

modified biochar particles into the base polymeric resin. While the FTIR spectra of the polymer nanohybrid and the composites were found to be similar, some distinct changes were recorded in the absorption bands corresponding to hydroxyl groups. The absorption bands for hydroxyl groups were observed to shift towards lower wavenumbers, specifically from 3456 to 3336 cm^{-1} after the formation of the polymer nanohybrid. The reason behind this could be due to the enhanced polar-polar interactions, viz. hydrogen bonding interactions between the polymer resin and the polar groups of modified biochar as well as bentonite nanoclay particles. In addition, IR peaks recorded in the frequency range of 1200-1300 cm^{-1} as well as 1600-1800 cm^{-1} attributed to C-O stretching and aromatic carbonyl stretching of modified biochar material, respectively. The findings reported that the intensity of C-O and C=O peaks became more pronounced with the introduction of the reinforcing agents, viz., bentonite nanoclay and modified biochar particles. This reaffirms the successful fabrication of the modified biochar/ bentonite clay/ poly(ester amide urethane) nanocomposite. Lastly, IR peaks observed in the frequency range of 2865-2943 cm^{-1} were noted as the symmetric and asymmetric sp3 C-H stretching vibrations of the polymer nanohybrid. **Figure 5.1. (c)** illustrated all the FTIR absorption peaks discussed elaborately above, for the polymer nanocomposites.

5.3.3.4. XPS analysis

This method plays a crucial role in providing valuable information about various variables, viz., elemental surface composition, chemical bonding, and functional moieties present in the polymer nanocomposites. A thorough examination of the XPS spectrum unveiled the prevalent presence of C, O, N, and Si as the prime elements, along with Al, Ca, Na, Mg, S, and P as the trace elements in the polymer nanocomposite material, as displayed in **Figure 5.2. (a)**. The atomic fractions of these elements were ascertained to be 0.65%, 0.06%, 0.1%, 0.07%, 0.47% and 0.25%, respectively. The existence of these elements signified the successful incorporation of bentonite nanoclay and modified biochar particles into the poly(ester amide urethane) matrix. A comprehensive evaluation was carried out to augment the understanding by assessing the high resolution spectra of O 1s, N 1s, C 1s, and Si 2p. Under this pretext, the C 1s spectrum underwent deconvolution, resulting in three distinguished peaks at 284.82 eV (attributed to C-H and C-C groups), 285.81 eV (assigned to C-O and C-N groups), and 287.44 eV (associated with C=O groups), as illustrated clearly in **Figure 5.2. (b)**. These peaks were assessed as representative peaks of

carbon bearing entities, viz., citric acid, hexamethylene diamine, modified biochar, glycerol, etc. In turn, the O 1s spectrum was deconvoluted into two prominent peaks alloted to C-O at 531.65 eV and C=O at 532.22 eV. This deconvolution further clarified the existence of oxygen bearing functional groups prevalent in PEAU-MBC/clay nanocomposite as illustrated in **Figure 5.2. (c)**. In turn, the N 1s peak spectrum underwent deconvolution into two major peaks at 400.15 eV and 399.12 eV, corresponding to N-H and N-C functional moieties, as enumerated in **Figure 5.2. (d)**.These spectral peaks conform to the fact that hexamethylenediamine and IPDI moieties exist in the PEAU-MBC/clay polymer nanocomposite. Interestingly, silicon displayed its corresponding spectral peak at 102.18 eV, thereby substantiating the fact that incorporation of bentonite nanoclay particles in the polymer nanocomposite took place successfully as shown in **Figure 5.2. (e)** [16]. Additionally, the XPS survey spectra for both the polymer nanocomposites bearing modified biochar particles and bentonite nanoclay particles were also conducted as displayed in **Figure 5.2. (f)** and **(g)**. The atomic fractions for both these composites were found out to be: Al- 0.51%, N- 2.76%, C- 68.81%, O- 27.67%, S- 0..24% and Al- 0.36%, C- 67.64%, O: 19.76%, Si- 8.43%, Ca- 0.01%, Fe- 0.21%, N- 3.22%, and Mg- 0.12%.

5.3.3.5. PXRD analysis

The PXRD analysis of the polymer nanocomposite aimed to evaluate the existence of interactions between the modified biochar as well as bentonite nanoclay particles and the poly(ester amide urethane) resin, as illustrated in **Figure 5.3.** All the studied polymer nanocomposites displayed XRD peaks within the range of 19.21-19.34°. These XRD peaks are indicative of the presence of PVA in the polymer matrix. In addition, the characteristic XRD peaks for bentonite nanoclay particles also fall within the same range as mentioned above. These XRD peaks refer to the (002) crystallographic plane of clay minerals. Moreover, studies have revealed that the nanoclay form typically results in broadening of the XRD peaks on ground of increased disorder and exfoliation of different layers of clay [21]. However, the XRD peaks of the modified biochar particles are found to be indistinguishable against the backdrop of the polymer matrix due to dilution effect. Since the modified biochar particles are well-dispersed and effectively integrated into the polymer matrix, this integration hindered the detection of specific XRD peaks on ground of potential dilution effects within the polymer matrix. Furthermore, the shift observed in

the values of XRD peaks of PVA provided insights into the crosslinked framework of the polymer nanocomposites along with the evolving structural elements of them.

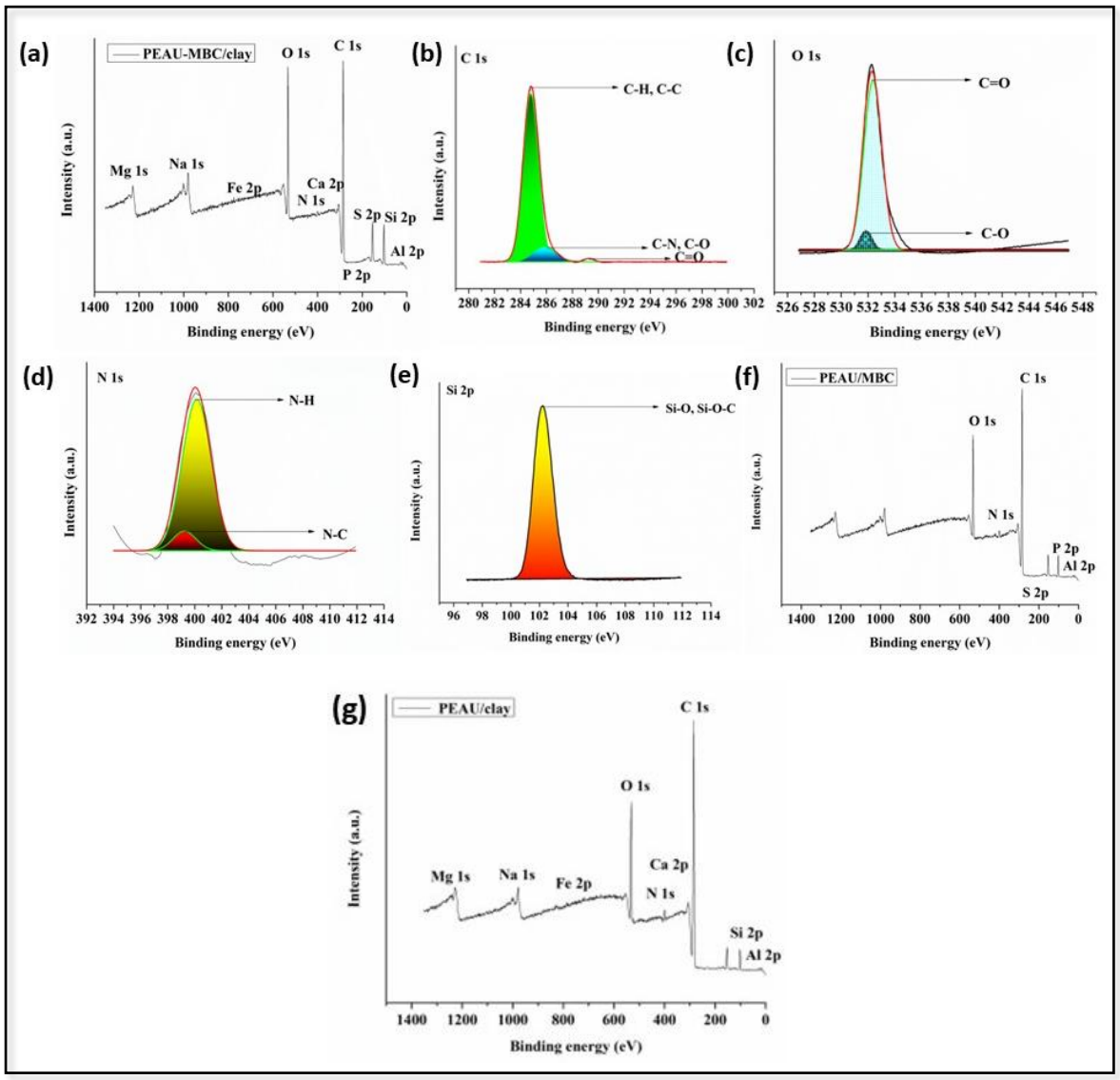

Figure 5.2. (a) XPS survey spectra, **(b)** C 1s, **(c)** O 1s, **(d)** N 1s, **(e)** S 2p high resolution spectra for PEAU-MBC/clay nanocomposite, and XPS survey spectra for **(f)** PEAU/ MBC, and **(g)** PEAU/ clay nanocomposites.

5.3.3.6. FESEM and EDX analyses

The FESEM study was carried out to evaluate the morphology, distribution and interactions of the polymer nanocomposites with modified biochar and bentonite nanoclay particles as the reinforcing agents, respectively. The FESEM images as shown in **Figure 5.4. (a)** exhibited the characteristic structure of the bentonite nanoclay particles in the form

of platelets or sheets. This illustrates the homogeneous distribution of these particles throughout the polymer matrix and therefore indicates effective incorporation into the

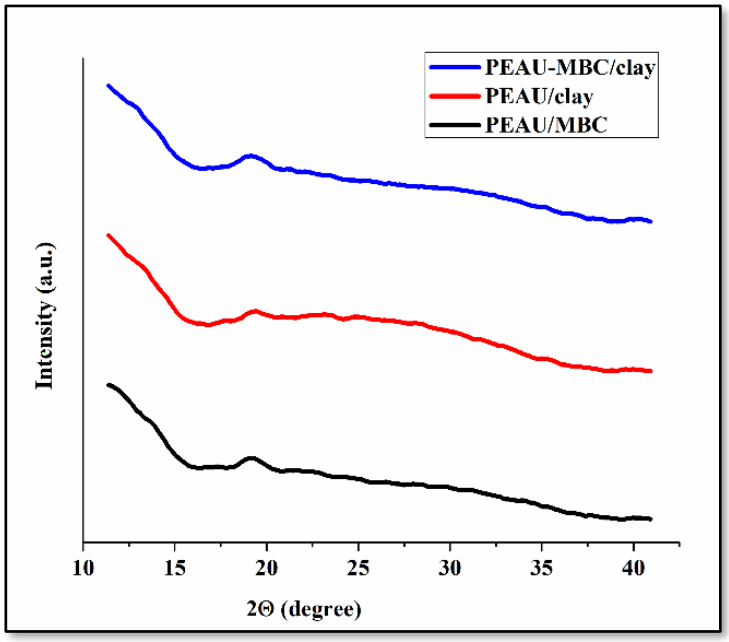

Figure 5.3. PXRD spectra of polymer nanocomposites integrated with modified biochar as well as bentonite nanoclay particles.

matrix, leading to successful fabrication of the polymer nanocomposite [25]. Similarly, the FESEM images as illustrated in **Figure 5.4. (b)** provided a detailed perspective on the even distribution of modified biochar particles within the poly(ester amide urethane) matrix. The presence of the spherical particles within the polymer surface confirmed the successful incorporation of biochar particles into the polymer matrix. Moreover, these images revealed the homogeneity of these particles, and a homogeneous distribution of particles is indeed desirable for achieving consistent properties in different applications. In addition, the FESEM images as presented in **Figure 5.4. (c)** provided a comprehensive assessment of the uniform distribution and integration of both modified biochar as well as bentonite nanoclay particles into the poly(ester amide urethane) matrix. The polymeric surface exhibited a heterogeneous texture with discernible clusters, indicative of the bentonite nanoclay and modified biochar particles. The modified biochar particles, displaying spherical morphology, were observed in conjunction with the platelet or sheet like structures of bentonite nanoclay particles. This overall combination contributed to the creation of an interconnected and well-dispersed network within the nanocomposite.

Additionally, elemental assessment of the polymer nanocomposites was performed using the EDX technique. This aimed at quantification and identification of various elements

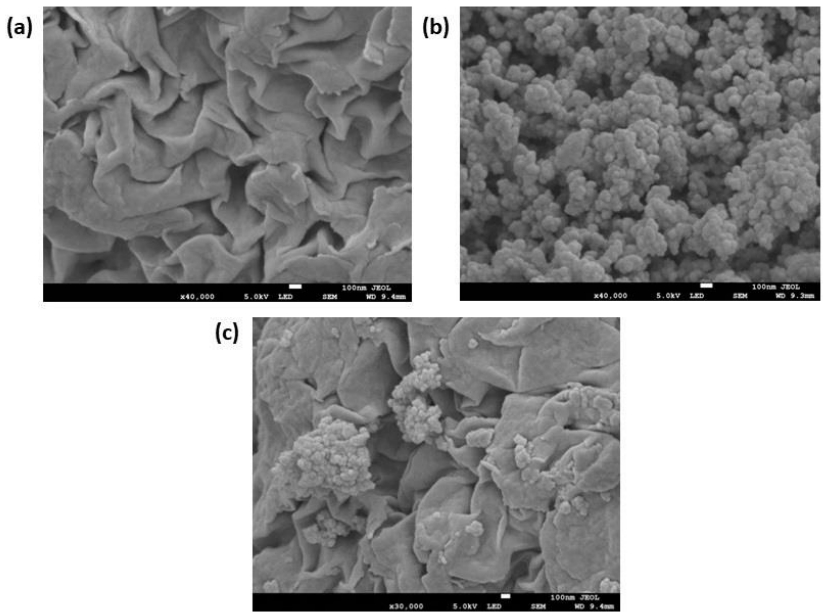

Figure 5.4. FESEM images of **(a)** PEAU/ clay, **(b)** PEAU/ MBC, and **(c)** PEAU-MBC/ clay materials.

present in these materials. **Figure 5.5.** enumerated the distribution of different elements of the polymer nanohybrid as well as modified biochar and bentonite nanoclay nanocomposites, along with the weight percentages of the detected elements which were determined to be: C- 49.01%, N- 8.15%, O- 38.75%, Mg- 0.03%, Na- 0.26%, Al- 0.23%, Si- 0.55%, P- 0.05%, Ca- 0.18% and S- 2.79%. The weight percentages of PEAU/clay and PEAU/MBC materials were ascertained to be: C- 44.95%, N- 7.95%, Na- 0.29%, O- 45.06%, Mg- 0.11%, Al- 0.26%, Ca- 0.15%, Si- 0.83%, Fe- 0.38% and C- 55.16%, N- 2.00%, O- 38.55%, P- 0.26%, S- 3.71%, Al- 0.31%, respectively. Moreover, the XPS and ultimate analyses provided consistent findings, thereby substantiating the results obtained through EDX analysis.

5.3.4. Mechanical properties

The mechanical properties portray a pivotal role in determining the overall applicability and performance of polymeric materials, signifying both versatility as well as durability. Polymer nanocomposites, incorporating nano-sized reinforcing agents, have been

recognized for their enhanced mechanical characteristics as compared to the unmodified counterparts. In this context, biochar, among other eco-friendly materials, has acquired

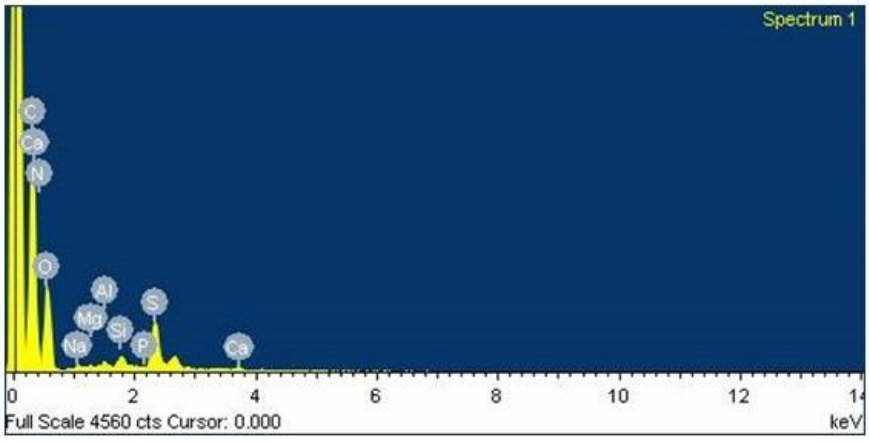

Figure 5.5. EDX map of PEAU-MBC/clay nanocomposite.

considerable attention as a potential reinforcing agent in polymer matrices from material scientists all across the globe. Accordingly, biochar particles derived from kraft lignin underwent modification using epichlorohydrin and triethylamine, were incorporated into poly(ester amide urethane) resin. Additionally, over the years, bentonite nanoclay has gained widespread use as a reinforcing agent in different polymer matrices, offering several advantages and increment to the functional and mechanical properties of the resulting nanocomposite materials. Likewise, bentonite nanoclay particles were also introduced into the polymer matrix to fabricate the polymer nanocomposite. The resulting modified biochar/ bentonite clay/ poly(ester amide urethane) nanocomposite exhibited significantly improved mechanical properties in contrast to modified biochar/ poly(ester amide urethane) and bentonite clay/ poly(ester amide urethane) composites, as detailed in **Table 5.4.** The stress-strain profiles are presented in **Figure 5.6.** Remarkably, a substantial enhancement in the mechanical properties was evident for PEAU-MBC/clay nanocomposite in comparison to the polymer nanocomposites PEAU/ clay and PEAU/ MBC at 0.5 wt% loading. It was noted that the elongation at break and tensile strength values for PEAU-MBC/clay nanocomposite was determined to be 2149% and 9.57 MPa, respectively. Correspondingly, this overall increase in the mechanical parameters of PEAU-MBC/clay nanocomposite material resulted in an improvement in the toughness variable, i.e., 87.45 MJ/m^3, derived from the integral area, beneath the stress-strain curves.

In a similar way, other mechanical variables, viz., scratch hardness, impact resistance, etc. showed improved results for PEAU-MBC/clay nanocomposite compared to other two polymer nanocomposites. Hence, these findings ultimately indicated that PEAU-MBC/clay nanocomposite exhibited superior mechanical toughness when compared to the parent poly(ester amide urethane) resin as well as other two polymer nanocomposites.

Table 5.4. Mechanical properties of the fabricated modified biochar/ bentonite clay/ poly(ester amide urethane) nanocomposite, modified biochar/ poly(ester amide urethane), and bentonite nanoclay/ poly(ester amide urethane) nanocomposites.

Sample	PEAU/ clay	PEAU/ MBC	PEAU-MBC/ clay
Tensile strength (MPa)	7.21 ± 0.68	8.45 ± 0.57	9.57 ± 0.61
Elongation at break (%)	3074 ± 2.83	2569 ± 1.17	2149 ± 0.86
Toughness (MJ/m^3)	98.22 ± 1.14	90.78 ± 2.54	87.45 ± 3.12
Impact strength (kJ/m)	21.7 ± 1.4	22.8 ± 2.2	22.7 ± 2.5
Scratch hardness (kg)	7.5 ± 0.5	8.0 ± 0.5	8.5 ± 0.5

The elevated tensile strength values observed in the polymer nanohybrid material can be ascribed to the fine surface area exhibited by the modified biochar particles along with their distinctive chemical structure. These factors in conjunction with homogeneous dispersion within the polymer matrix also aid in enhancing the tensile strength values. Furthermore, the considerable surface area of modified biochar particles, along with its array of different functional groups positions it as a highly effective reinforcing agent. Conversely, bentonite nanoclay particles also help in enhancing the tensile strength values by reinforcing the polymer matrix. These clay particles tend to create a network within the polymer matrix, thereby providing structural support that helps in resisting deformation, and overall help in enhancing the strength of the material [21]. Additionally, these clay

particles help in improving the flexural strength, along with the impact resistance parameters of PEAU-MBC/clay nanocomposite by absorbing as well as distributing the impact energy, thereby reducing the risk of fractures or cracks when the material is subjected to any sudden forces. Overall, both these reinforcing agents help in imparting rigidity and increased stiffness to the polymer matrix, making the resulting polymer nanocomposite more resistant and robust to deformation.

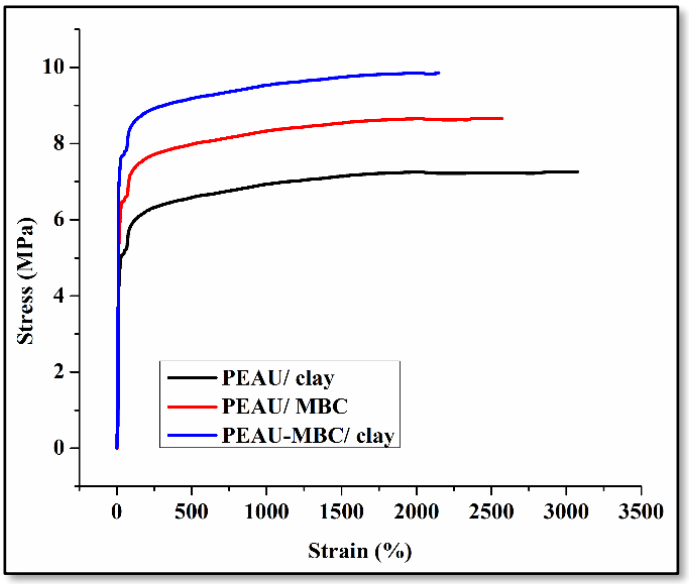

Figure 5.6. Stress-strain profiles for polymer nanocomposites.

Nonetheless, the polar functional groups present within the polymer nanocomposite involve in various interactions, viz., dipole-dipole as well as hydrogen bonding interactions, with the urethane, carboxyl, and hydroxyl groups present in the polymer matrix during the *in-situ* fabrication method. These forces of interactions contribute to augment the physico-mechanical interlocking process via chain entanglement mechanism within the polymer matrix, resulting in a reduction in the free volume as well as enhanced rigidity values [17].

5.3.5. Thermal properties

The evaluation of thermal durability parameter is of utmost importance in assessing the thermal stability as well as the degradation properties of various polymer nanocomposites intended for usage in various applications. Under this context, various features, viz., the degradation behavior and the thermal stability of all the formulated polymer

nanocomposites underwent critical analysis via TG. The corresponding TG thermograms, accompanied by their derivative curves, viz., dTG for both the polymer nanocomposites bearing modified biochar and bentonite nanoclay particles as the reinforcing agents, as well as PEAU-MBC/clay nanocomposite, as illustrated in **Figure 5.7. (a) a**nd **(b)**. In turn, the comprehensive information, viz., onset temperature, peak degradation temperature at 600 °C, and onset temperature has been compiled in **Table 5.5.** The analysis revealed that PEAU-MBC/clay nanocomposite exhibited thermal stability up to temperature value of 205.83 °C (T_{ON} temperature), in comparison to the other two polymer nanocomposite which demonstrated values of 203.45 °C (PEAU/ clay) and 204.80 °C (PEAU/ MBC). Moreover, all the TG modified thermograms, for PEAU-MBC/clay nanocomposite as well as other polymer nanocomposites, manifested a two-step degradation pattern similar to that observed in the parent poly(ester amide urethane) resin. This suggests that the incorporation of both the reinforcing agents, viz., biochar and bentonite nanoclay particles did not significantly influence the overall structural characteristics of the polymer nanohybrid material. However, notable variations were recorded in the peak degradation temperatures within each step of degradation of PEAU-MBC/clay nanocomposite.

The peak temperature associated with the initial step of degradation, i.e. 268.14 °C, attributed to the existence of different labile linkages, viz., ester moieties as well as aliphatic segments in PEAU-MBC/clay nanocomposite. The increment in the degradation temperature of PEAU-MBC/clay nanocomposite in comparison to the other two polymer nanocomposites outline the presence of various polar functional moieties, which facilitate the formation of a greater number of labile linkages during the course of fabrication. Bentonite nanoclay particles aid in enhancing thermal stability via different mechanisms. Its layered structure creates a barrier effect, thereby impeding the diffusion of various gases and other decomposition products during the heating process and slowing down the process of degradation. The high surface area of bentonite nanoclay particles also facilitates effective heat absorption and dissipation, thereby reducing the temperature fluctuations within PEAU-MBC/clay nanocomposite during the thermal events. In addition, the nanoclay particles promote the formation of a char layer which is protective in nature, acting as a physical barrier and further contributing to thermal stability during the thermal decomposition process [26]. Correspondingly, modified biochar, inherently exhibiting remarkable thermal stability, serves as strong evidence of its robustness and

heat resistant capability, a fact supported by numerous studies. In a similar way, the peak temperature of the second step of thermal degradation, associated with the existence of urethane, amide, and aromatic entities in the polymer matrix, was observed at 455.23 °C for PEAU-MBC/clay nanocomposite in comparison to the other polymer nanocomposites (PEAU/ clay: 421 °C and PEAU/ MBC: 436 °C). Hence, based on these findings, it can be concluded that the thermal stability of PEAU-MBC/clay nanocomposite surpasses that of other polymer nanocomposites as well as bare poly(ester amide urethane) resin, with an increase in thermostability corresponding to incorporation of both modified biochar and bentonite nanoclay particles into the polymer matrix. This assertion is substantiated by the analysis of char weight residues at 600 °C, revealing percentages of 30.14%, 31.09%, and 31.52% for PEAU/ clay, PEAU/ MBC and PEAU-MBC/ clay, respectively.

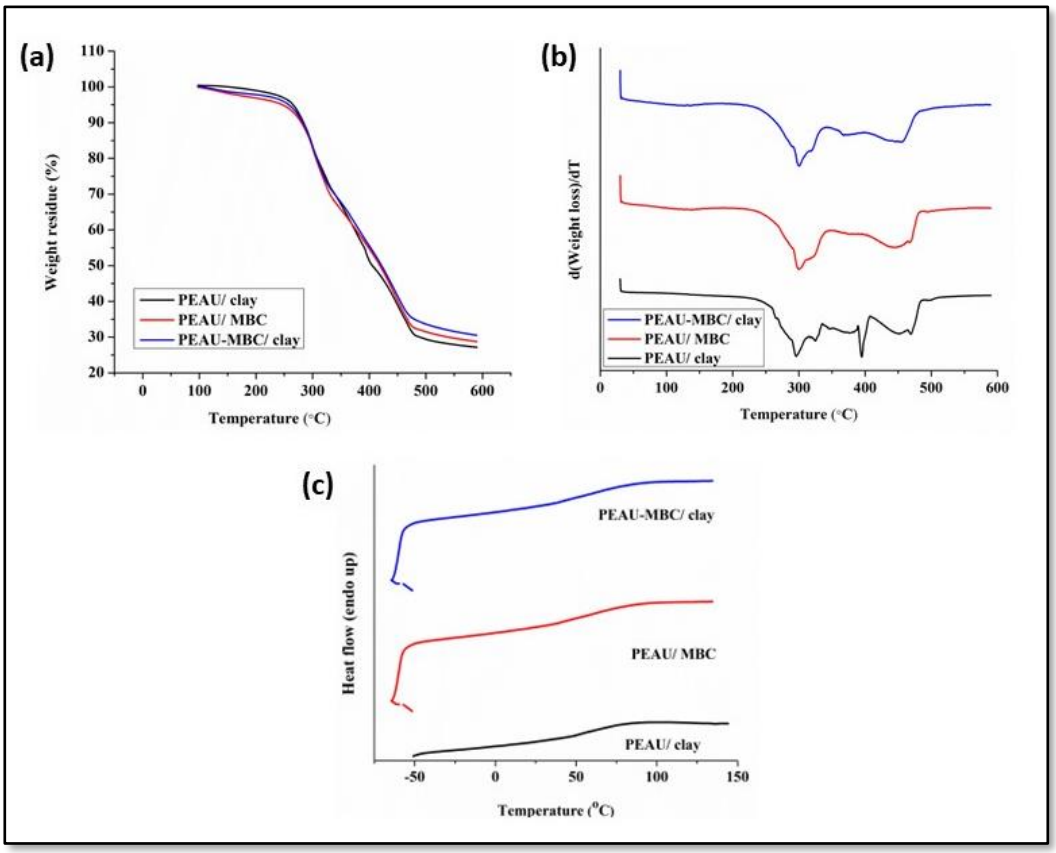

Figure 5.7. (a) TGA, **(b)** dTG, and **(c)** DSC profiles of polymer nanocomposites.

DSC studies were carried out to ascertain the T_g values of PEAU-MBC/clay nanocomposite, depicted in **Figure 5.7. (c)** revealing a temperature range of 81-84.56 °C. Notably, the incorporation of modified biochar and bentonite nanoclay particles led to an

increase in the T_g values, from 81 °C (PEAU/ clay) and 83.12 °C (PEAU-MBC) to 84.56 °C for PEAU-MBC/clay nanocomposite. This observed increment can be attributed to a substantial rise in the crosslinking values, resulting from enhanced intermolecular forces between the polymer matrix and the modified biochar as well as bentonite nanoclay particles [13, 14]. Consequently, it led to restricted mobility and reduction in the free volume, causing an elevation in T_g values.

Table 5.5. Thermal degradation variables for fabricated modified biochar/ bentonite clay/ poly(ester amide urethane), modified biochar/ poly(ester amide urethane), and bentonite nanoclay/ poly(ester amide urethane) nanocomposites.

Variables	PEAU/ clay	PEAU/ MBC	PEAU-MBC/ clay
T_{on} (°C)	203.45	204.80	205.83
1st stage degradation peak temperature (°C)	264.12	265.20	268.14
2nd stage degradation peak temperature (°C)	421	436	455.23
Weight residue (%) at 600 °C	30.14	31.09	31.52
Glass transition temperature, T_g (°C)	81	83.12	84.56

5.3.6. Biodegradation study

5.3.6.1. Microbial growth study

An investigation was conducted to assess the biodegradability of the polymer nanocomposites, through accelerated biodegradation testing method. The focus was on evaluating their effectiveness as environmentally friendly materials by targeting a specific bacterial strain, *Bacillus subtilis*. The optical values were monitored over time in the presence of these polymer nanocomposite materials. Remarkably, PEAU-MBC/clay nanocomposite material showed higher absorbance values, as detailed extensively in

Figure 5.8. (a). A discernible trend emerged, revealing a gradual increase in the optical values associated with PEAU-MBC/clay nanocomposite, in comparison to the other polymer nanocomposite materials. This suggested enhanced biodegradability associated with an elevated abundance of both modified biochar and bentonite nanoclay particles. The inclusion of both these reinforcing agents, featuring diverse polar functional moieties, facilitated interactions with different polar groups in the polymer matrix. This led to the formation of different labile linkages, viz., ester connectivity as well as hydrogen bonding linkages. In consequence, these additional linkages in PEAU-MBC/clay nanocomposite underwent hydrolysis by the *Bacillus subtilis* bacterial strain, causing massive surface erosion and thereby accelerating the biodegradation rate compared to the poly(ester amide urethane) alone. The weight loss profiles, as elucidated in **Figure 5.8. (b)**, highlighted the point that the presence of both the reinforcing agents, viz., modified biochar as well as bentonite nanoclay particles correlated with a rise in the hydrolysable linkages within PEAU-MBC/clay nanocomposite, resulting in a proportional acceleration of the rate of

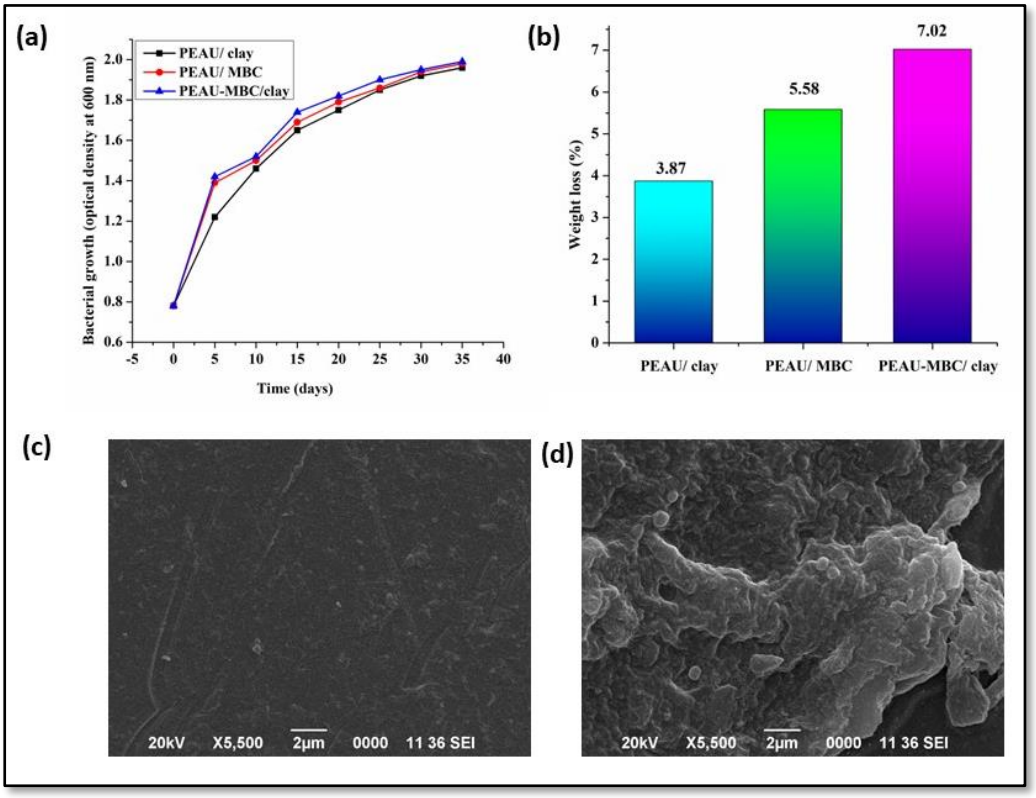

Figure 5.8. (a) Bacterial growth curves presented in terms of optical density as a function of time, **(b)** weight loss (%) of polymer nanocomposites after exposure to bacterial degradation, SEM images of PEAU-MBC/ clay **(c)** control specimen, and **(d)** biodegraded by bacterial strain, *Bacillus subtilis.*

biodegradation and significant weight loss. The SEM images in **Figure 5.8. (c)** and **(d)** emphasized the extent or magnitude of bacterial growth (*Bacillus subtilis*) on PEAU-MBC/clay nanocomposite. In turn, these images were subsequently compared with a control sample lacking any bacterial strain.

5.3.6.2. Soil burial study

Another aspect of the biodegradability assessment involved conducted a soil burial test by exposing the samples under consideration to real field conditions under the influence of soil bacteria. Initially, the chemical composition of the soil organic matter was thoroughly examined using a CHN analyzer, revealing the primary components of the soil (carbon: 6.15%, hydrogen: 0.5%, and nitrogen: 0%). Additionally, the soil pH was determined to be moderately alkaline (pH: 8.14). To evaluate the expanse of surface degradation and assess the changes in surface morphology, the gravimetric weight loss profiles were measured, and the SEM image studies were conducted. **Figure 5.9. (a)** illustrates the weight loss (%) study for the polymer nanocomposites, viz., PEAU-MBC/clay PEAU/ clay and PEAU/ MBC over 60-days period. The bar graph indicates that PEAU-MBC/clay nanocomposite exhibited the highest weight loss (%) values in comparison to the other polymer nanocomposites (PEAU/ clay and PEAU/ MBC). This observation can be attributed to the fact that the presence of both reinforcing agents enhances the material's interaction with soil microbes, promoting biodegradation. The modified biochar particles provided a conducive environment for microbial colonization and activity, thereby accelerating the breakdown of organic components in PEAU-MBC/clay nanocomposite. Similarly, the bentonite nanoclay particles contributed to the material's biodegradability by increasing the surface roughness and providing additional sites for enzymatic action as well as microbial attachment. In turn, the intercalation of bentonite nanoclay particles within PEAU-MBC/clay nanocomposite facilitated nutrient as well as water absorption, further promoting microbial activity and biodegradation. Moreover, the synergistic effects of both these reinforcing agents, resulted in enhancing the overall stability of PEAU-MBC/clay nanocomposite in soil, preventing premature degradation and ensuring sustained release of degradation byproducts over time. This prolonged exposure to soil conditions allowed for thorough assessment of biodegradability and environmental impact. These findings align with previous literature reports, emphasizing that the surface attack is the primary mode employed by bacteria in the degradation process, resulting in

substantial weight loss over time.

The SEM analyses were conducted on the nanocomposite material exposed to soil to assess its morphology. **Figure 5.9. (b)** and **(c)** illustrated the differences between the untreated polymer specimen and PEAU-MBC/clay nanocomposite subjected to soil microbes. The examined specimen exhibited significant roughness compared to the smooth texture of the control sample, indicating extensive degradation and surface erosion caused by soil microbes. These findings align completely with the gravimetric weight loss profiles, confirming the biodegradability of the synthesized polymer nanocomposite demonstrated in both the biodegradation assays.

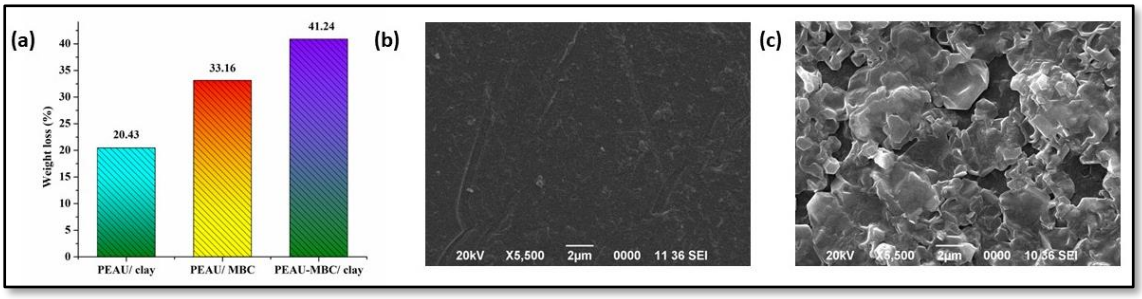

Figure 5.9. (a) Weight loss (%) profile; SEM images of PEAU-MBC/ clay **(b)** control specimen and **(c)** biodegraded by soil microbes against exposure time.

5.3.7. Heavy metal ion adsorption

To evaluate the effectiveness of the polymer nanocomposite as adsorbent, heavy metal ion adsorption tests were carried out. The polymer nanocomposite, incorporating modified biochar and bentonite nanoclay particles, was chosen to serve as an efficient adsorbent for heavy metal ion removal on ground of its increased surface area and porosity. Correspondingly, both these reinforcing agents provided active sites as well as chemical affinity for heavy metal ions, thereby allowing for selective adsorption. An experiment was conducted in a liquid phase to investigate the adsorption characteristics of PEAU-MBC/clay nanocomposite towards the heavy metal ions, viz., Pb(II), Cu(II) and Zn(II) ions. Overall, the polymer nanocomposite (PEAU-MBC/ clay) was utilized for conducting all the adsorption assessments. In turn, it is well-recognized that the efficiency of heavy metal ion removal depends on various factors, viz., preliminary concentration of the metal ions, temperature, pH of the solution containing these heavy metal ions, adsorbent dosage,

adsorption time, etc. [27] A thorough investigation into the impact of these variables on heavy metal ion adsorption was conducted to optimize the adsorption process.

5.3.7.1. Effect of adsorbent dose

The impact of the adsorbent on the capacity for heavy metal ion adsorption was assessed to determine the optimal dosage of polymer nanocomposite required for the removal of each metal ion as illustrated exclusively in **Figure 5.10. (a)** and **(b)**. Additionally, it is clearly observed from **Figure 5.10. (a)** and **(b)** that there is a trend of increasing removal efficiency with higher polymer nanocomposite loading, while the adsorption capacity exhibited a decline in its values. The rise in the removal efficacy parameter of Pb(II), Cu(II) and Zn(II) ions with increased polymer nanocomposite loading suggested an augmentation in the availability of adsorption sites. However, the observed increment in PEAU-MBC/clay nanocomposite loading with a progressive reduction in the adsorption competency parameter could be attributed to the potential saturation of the adsorption sites during the process of adsorption. In our study, the maximum removal efficiency (%) for Pb(II), Zn(II) and Cu(II) ions were determined to be 80.38%, 76.06%, and 70.80%, respectively, using adsorbent dosages of 50 mg, 60 mg, and 70 mg. Consequently, by considering these findings, the adsorbent dosages for the heavy metal ions were optimized to ensure the removal of more than 80% of the heavy metal ions at a concentration of 200 ppm. Additionally, based on the impact of adsorbent dosages, the adsorption capacities, expressed in mg/g, for the three heavy metal ions were measured as 47.05 mg/g for Pb(II), 21.85 mg/g for Cu(II), and 40.63 mg/g for Zn(II). This outcome is attributed to the higher affinity exhibited by Pb(II) ions towards carboxyl groups as compared to the other two heavy metal ions, viz., Zn(II) and Cu(II).In turn, Pb(II) ions outcompete Cu(II) and Zn(II) ions for adsorption sites on PEAU-MBC/clay nanocomposite due to their faster kinetics or higher affinity, resulting in preferential adsorption of Pb(II) over the other ions [28]. Overall, it can be stated that the specific adsorption behavior of lead compared to zinc and copper by PEAU-MBC/clay nanocomposite depended on the interplay of a wide variety of factors including chemical properties, competition for adsorption sites, surface chemistry, etc.

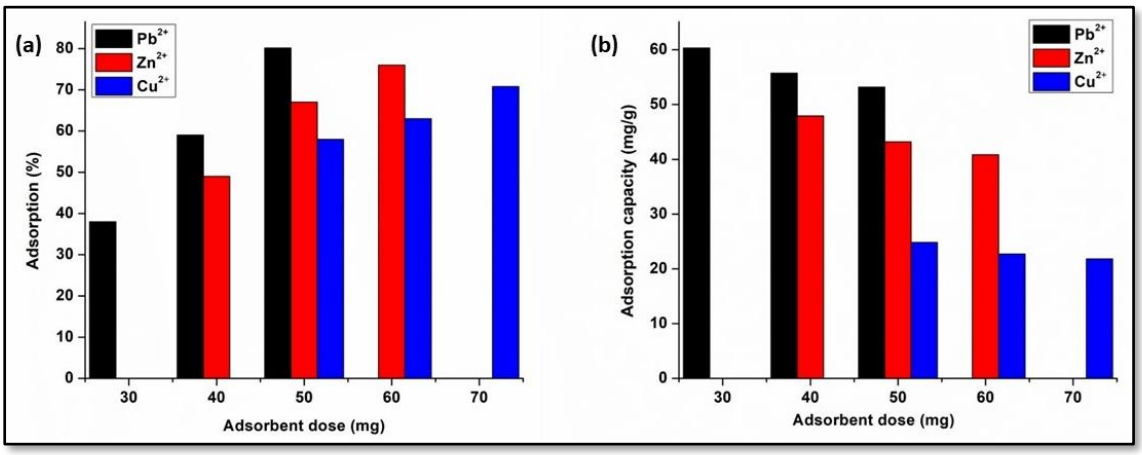

Figure 5.10. Effect of adsorbent dose on **(a)** adsorption (%), and **(b)** adsorption capacity (mg/g) for Pb(II), Zn(II) and Cu(II) ions by PEAU-MBC/ clay material.

5.3.7.2. Effect of preliminary heavy metal ion concentration

The consequence of varying heavy metal ion concentrations, ranging from 20 ppm to 200 ppm, on the adsorption performance of the polymer nanocomposite was closely investigated while carrying out the maintenance of the optimized amount of adsorbent material during the adsorption test. As depicted in **Figure 5.11.**, it is conclusive that increasing the heavy metal ion concentration resulted in higher adsorption amounts [22]. Moreover, a corresponding increase in the adsorption capacity parameter was observed, increasing from 22.46 mg/g to 53.37 mg/g for Pb(II), 5.23 mg/g to 21.17 mg/g for Cu(II), and 11.30 mg/g to 40.62 mg/g for Zn(II) ions, respectively. This phenomenon can be explained by the fact that at lower heavy metal ion concentration of 20 ppm, there was an abundance of active adsorption sites contributing to a greater overall adsorption percentage. Conversely, with the increment in the heavy metal ion concentration, there is decrease in the availability of the active adsorption sites on the surface of the polymer nanocomposite. As a result, a lower adsorption percentage was observed at higher heavy metal ion concentrations [19, 22].

5.3.7.3. Effect of contact time

Figure 5.12. demonstrated how the adsorption capacity variable of the heavy metal ions, viz., Pb, Zn, and Cu by PEAU-MBC/clay nanocomposite changes over time. The equilibrium time for adsorption was determined to be 180 minutes for all the heavy metal

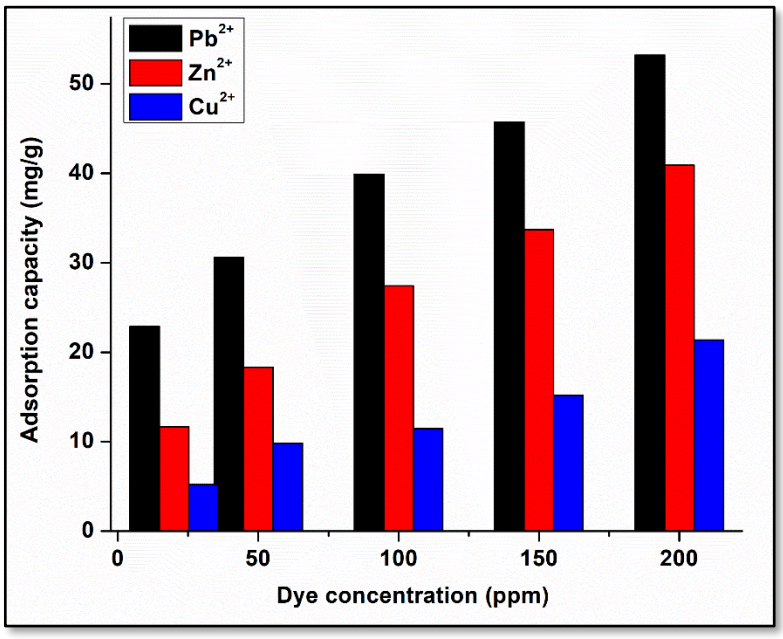

Figure 5.11. Effect of dye concentration on adsorption capacity (mg/g) for Pb(II), Zn(II) and Cu(II) ions by PEAU-MBC/ clay material.

ions, viz., Pb(II), Zn(II), and Cu(II) ions. After this time, the heavy metal ions adsorption levelled off, indicating that equilibrium had been reached. Interestingly, the rate of adsorption is more rapid in the initial stages compared to the period leading up to equilibrium. This suggested that initially, there might be existence of electrostatic interactions between the heavy metal ions as well as the charged active locations of the polymer nanocomposite. However, after a short period of time, the number of active adsorption sites decreased for the heavy metal ions, resulting in a reduction in the adsorption rate. Subsequently, there is a mass transfer of heavy metal ions involving dipole-dipole, hydrogen bonding, and other forces of interactions. These findings are completely consistent with previous studies [22, 23]. This outcome suggested that the fabricated polymer nanocomposite can attain equilibrium adsorption within a short time frame, thereby highlighting its practical utility as an effective adsorbent material.

5.3.7.4. Effect of temperature

The temperature parameter portrays a significant role in influencing the process of adsorption. **Figure 5.13.** illustrated the fact that the adsorption capacity of PEAU-MBC/clay nanocomposite for all three heavy metal ions, viz., Pb(II), Zn(II), and Cu(II)

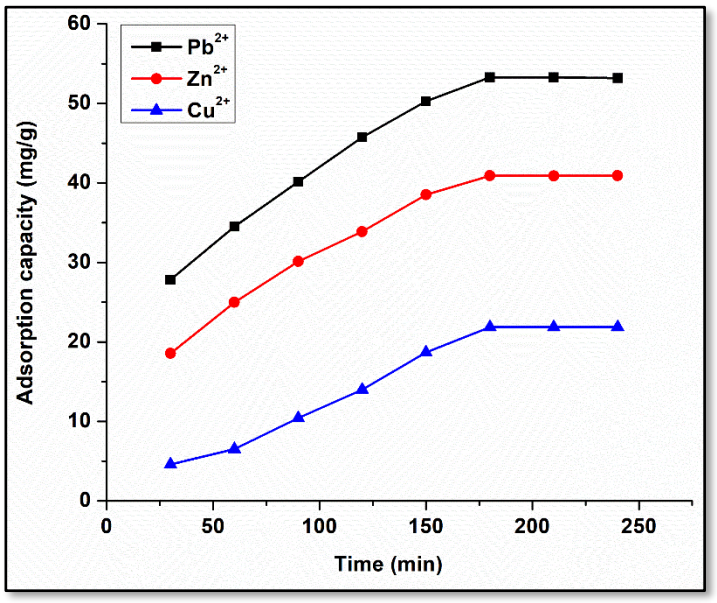

Figure 5.12. Effect of contact time on adsorption capacity (mg/g) for Pb(II), Zn(II) and Cu(II) ions by PEAU-MBC/ clay material.

notably improved as temperature variable increased from 303 K (room temperature) to 323.15 K. It could be suggested that with elevation in temperature parameter, more heavy metal ions acquire the requisite energy required to carry out interactions with the negatively charged active locations of the adsorbent material. Additionally, temperature elevation aids in enhancing the diffusion rates by carrying out reduction in the viscosity of the solutions, thereby leading to improved adsorption rates [23, 25]. This indicated the endothermic nature of the adsorption process.

5.3.7.5. Effect of pH

The pH of the solution plays a crucial role in influencing the adsorption performance, thereby affecting both the behavior of heavy metal ions viz., Pb(II), Zn(II), and Cu(II) in aqueous solutions as well as the physicochemical features of the adsorbent material, viz., the polymer nanocomposite material. The impact of pH on the heavy metal ion adsorption by the polymer nanocomposite was examined across a pH ambit of 2 - 10, with the results presented in **Figure 5.14**. It was observed that the adsorption capacity increased as the values of the solution pH rose from 2 to 6, but eventually decreased thereafter. The lower adsorption performance recorded at pH < 6 can be attributed to the competitive interaction

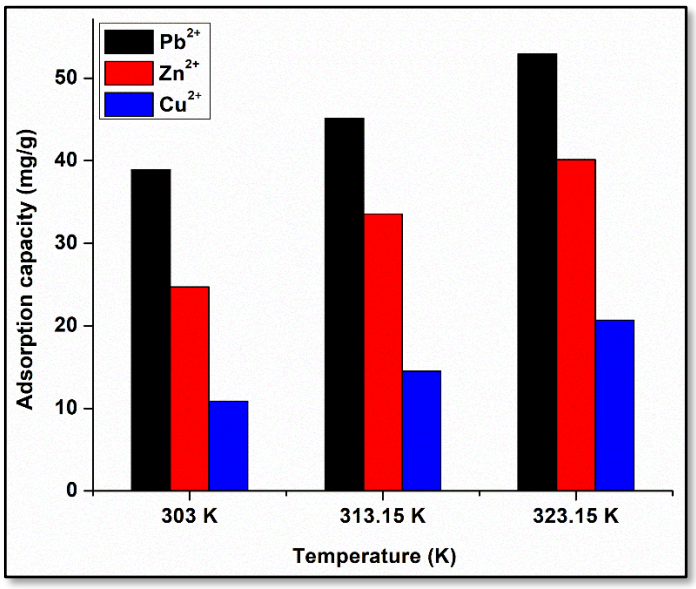

Figure 5.13. Effect of temperature on adsorption capacity (mg/g) for Pb(II), Zn(II) and Cu(II) ions by PEAU-MBC/ clay material.

existing between the large quantity of H^+ ions as well as the heavy metal ions, which compete for conducting interactions with the negatively charged active locations or sites of the adsorbent material [27]. Moreover, as the pH values increased, a notable improvement in the pH values on ground of reduction in the H^+ ions in the solution, thereby decreasing competition between the H^+ ions as well as the heavy metal ions. However, further increment in the solution pH values led to a decrease in the adsorption capacity values likely due to the abundance of OH^- ions in the medium, which resulted in enhancing the affinity of the adsorbate towards them, followed by decreased efficiency of the adsorbent material for heavy metal ion binding [22].

5.3.8. Kinetics study

Adsorption kinetics is considered as an important parameter for predicting and understanding the adsorption process, as it aids in determining the rate at which adsorption process takes place. Moreover, in order to understand the adsorption mechanism, thorough investigation of the PFO model, PSO model, and IPD model was conducted in an elaborate way as mentioned in **Chapter 4**. In turn, **Chapter 4**, highlighted the linear versions of these models, represented by equations **4.3**, **4.4**, and **4.5**, respectively. In this context, **Figure 5.15.** (**(a)**, **(b)**, and **(c))** illustrates the linear plots showing $\log(q_e\text{-}q_t)$ against t, (t/q_t)

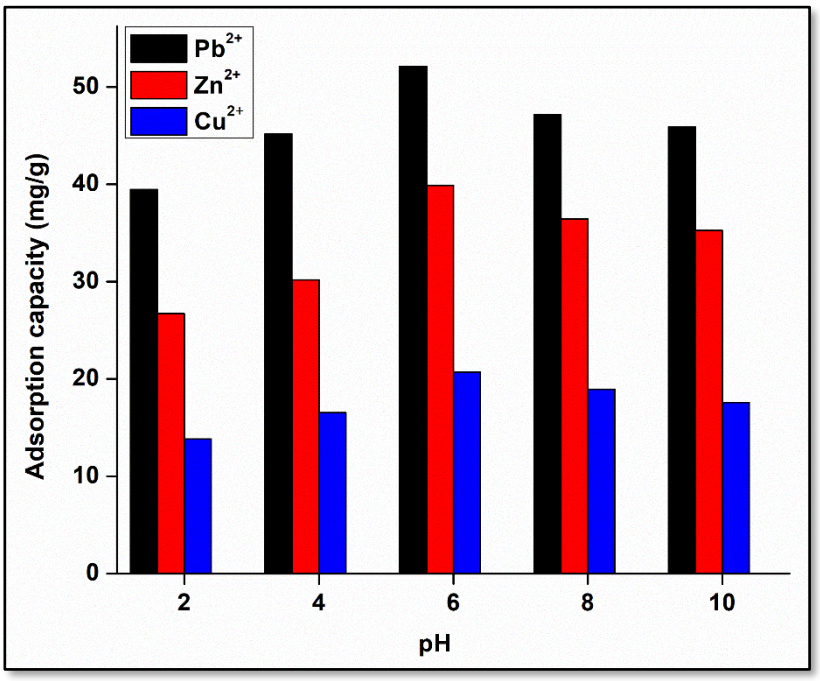

Figure 5.14. Effect of pH on adsorption capacity (mg/g) for Pb(II), Zn(II) and Cu(II) ions by PEAU-MBC/ clay material.

against t for PFO and PSO models, respectively and q_t against $t_{1/2}$ for IPD model. The close proximity of the linear correlation coefficient denoted as R^2, to unity indicates a strong fit. In this context, the PSO model yielded correlation coefficients of 0.99, 0.99, and 0.99, for Pb(II), Zn(II), and Cu(II) ions, respectively. Conversely, for PFO model, the correlation coefficients for Pb(II), Zn(II), and Cu(II) ions were found to be lower, at 0.58, 0.60, and 0.58, respectively. These correlation coefficient values suggested that the PSO model is more reliable, indicating that the adsorption mechanism is exclusively based upon the chemisorption process, occurring via electrostatic or ionic forces of interactions, between the adsorbate and adsorbent moieties [29]. Additionally, this step is considered as the rate determining step of this adsorption mechanism. The results obtained by exploring different kinetic models are summarized in **Table 5.6.** Additionally, the kinetics data underwent analysis using the IPD model. According to the criteria of this model, a larger intercept (c) indicates a greater boundary thickness or layer. Furthermore, if this process is involved in the adsorption mechanism, the plot of q_t against $t_{1/2}$ should show a linear relationship. Moreover, if this adsorption process significantly influences the rate determining step, then the plot should pass through the origin. However, the presence of the multilinear plots

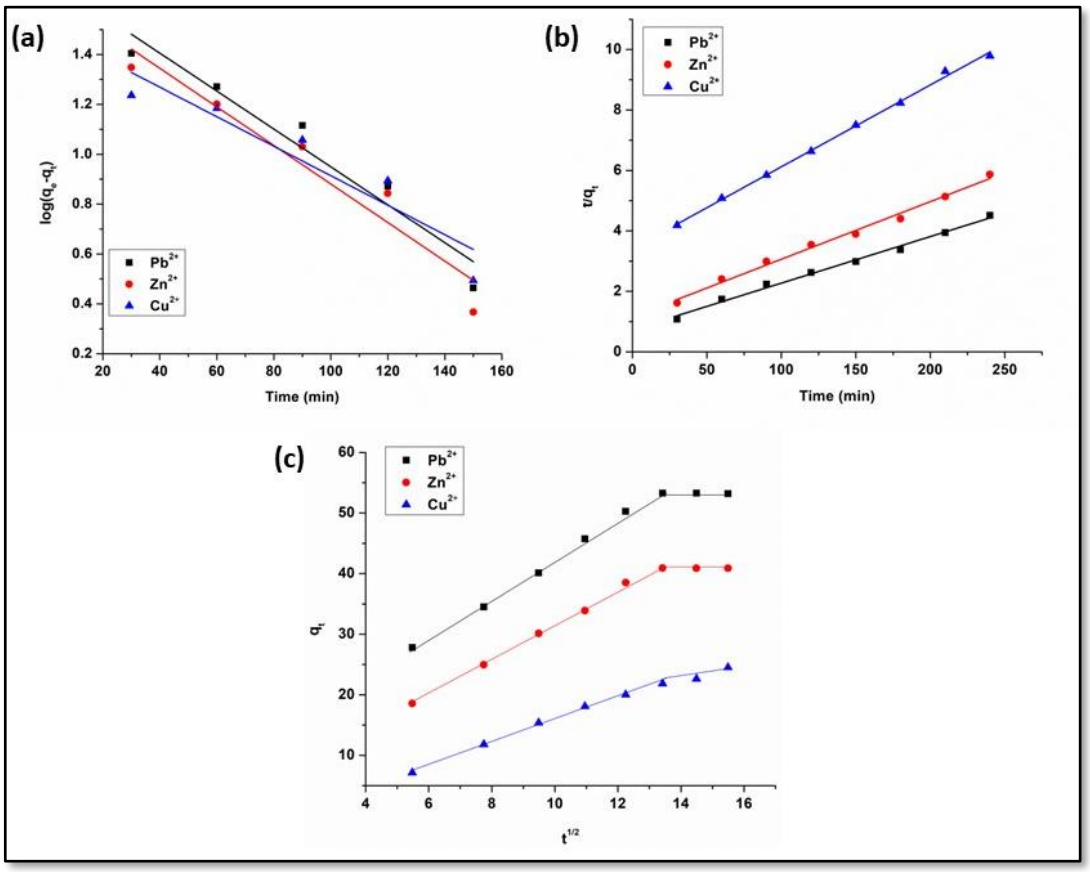

Figure 5.15. (a) PFO kinetics model, **(b)** PSO kinetics model, and **(c)** IPD model for Pb(II), Zn(II) and Cu(II) ions by PEAU-MBC/ clay material.

suggests that more than one process operates simultaneously during the adsorption process.

5.3.9. Isotherm study

The adsorption isotherm provides insight into the interactions between the adsorbent and adsorbate molecules. To assess the adsorption mechanism of heavy metal ions, we employ the Freundlich, Langmuir, and Temkin adsorption isotherms, as illustrated in **Figure 5.16. (a)**, **(b)**, and **(c)**. The mathematical expressions for these adsorption isotherms are represented by equations **4.6**, **4.7**, and **4.8**, respectively as explained in detail in **Chapter 4**. The results acquired from the intercepts and slopes of the linear plots for the Langmuir (C_e/q_e against C_e), Temkin (q_e against ln C_e), and Freundlich (ln q_e against ln C_e) adsorption isotherms are summarized in **Table 5.7.** The Temkin and Freundlich isotherm models displayed a poor fit with the data, indicating monolayer adsorption during the uptake of

Table 5.6. The kinetics variables for adsorption of Pb(II), Zn(II), and Cu(II) ions on PEAU-MBC/clay nanocomposite.

Model	Kinetics parameters	Pb^{2+} ions	Zn^{2+} ions	Cu^{2+} ions
PFO	k_1	4.54×10^{-1}	4.78×10^{-1}	4.15×10^{-1}
	R^2	0.58	0.60	0.58
PSO	k_2	7.42×10^{-2}	7.15×10^{-2}	7.34×10^{-2}
	R^2	0.99	0.99	0.99
IPD	k_{ip}	5.45	4.28	4.19
	c	35.71	34.52	35.89
	R^2	0.74	0.71	0.75

heavy metal ions, viz., Pb(II), Zn(II), and Cu(II) ions. Conversely, the Langmuir adsorption isotherm showed excellent alignment, with a very high correlation factor of for all the three heavy metal ions, viz., Pb(II), Zn(II), and Cu(II) ions. This suggested that the adsorption of the heavy metal ions onto the surface of PEAU-MBC/clay nanocomposite invoked binding energies which were uniform in nature, and distributed homogeneously across the surface of the material. Additionally, this adsorption process involved physisorption within the layers of the polymer nanocomposite, inherently monolayer by nature. All these findings are found to be consistent with the previous reports. In summary, the Langmuir adsorption isotherm emerges as the optimal model for evaluating the heavy metal ion adsorption behavior for all three heavy metal ions, viz., Pb(II), Zn(II), and Cu(II) ions [30].

5.4.0. Regeneration of adsorbent

To evaluate the potential for reusing the adsorbent material in heavy metal ions (Pb(II), Zn(II), and Cu(II) ions) adsorption, the polymer nanocomposite material was retrieved using a straightforward process of filtration, followed by thorough washing with deionized water and 0.1 N HCl solution. Afterward, the collected samples of polymer nanocomposite

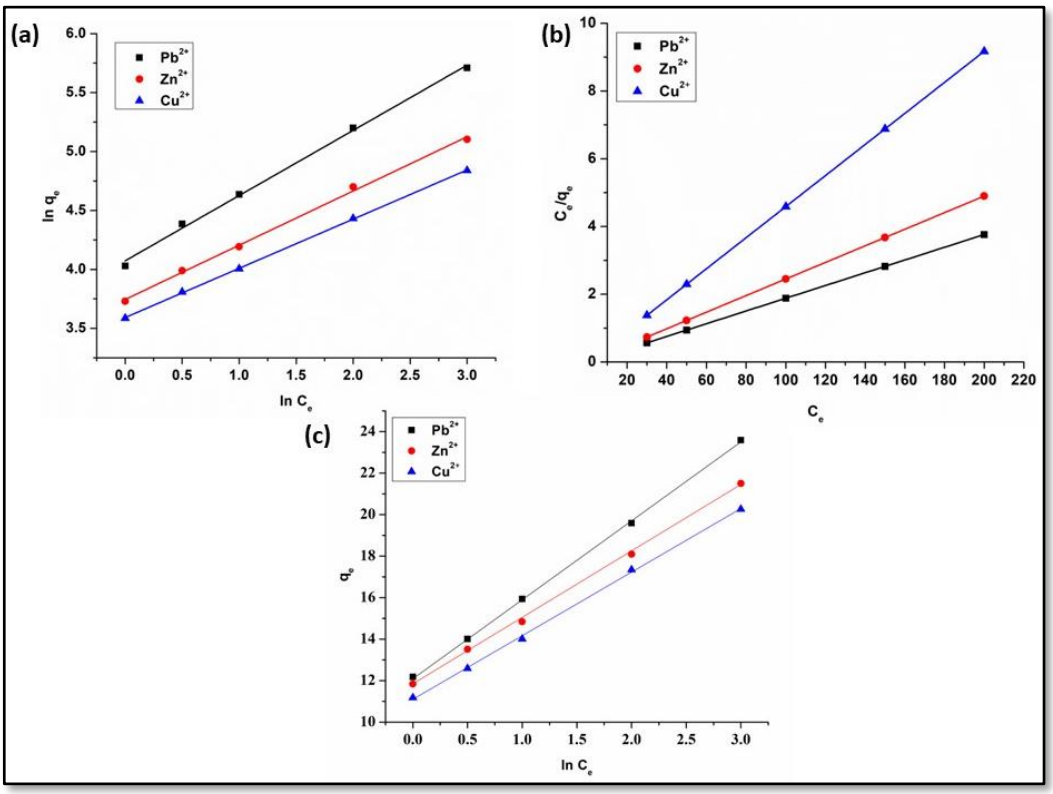

Figure 5.16. (a) Freundlich isotherm, **(b)** Langmuir isotherm, **(c)** Temkin isotherm for Pb(II), Zn(II), and Cu(II) ions by PEAU-MBC/ clay material.

Table 5.7. The isotherm parameters for adsorption of Pb(II), Zn(II), and Cu(II) ions on polymer nanocomposite.

Model	Isotherm variables	Pb^{2+} ions	Zn^{2+} ions	Cu^{2+} ions
Freundlich isotherm	n	2.17	2.32	2.45
	k_f	22.53	25.12	24.42
	R^2	0.98	0.98	0.97
Langmuir isotherm	Q_m	235.37	194.98	132.75
	k_l	2.35	3.56	3.97
	R^2	0.99	0.99	0.99
Temkin isotherm	b	1213.61	1048.30	1010.56
	k_m	47.08	38.89	39.54
	R^2	0.97	0.96	0.96

were dried at temperatures ranging from 100 to 105 °C. This recovery procedure was iterated five times for consecutive adsorption experiments. Therefore, the findings as illustrated in **Figure 5.17.** revealed a favorable capacity for recovery.

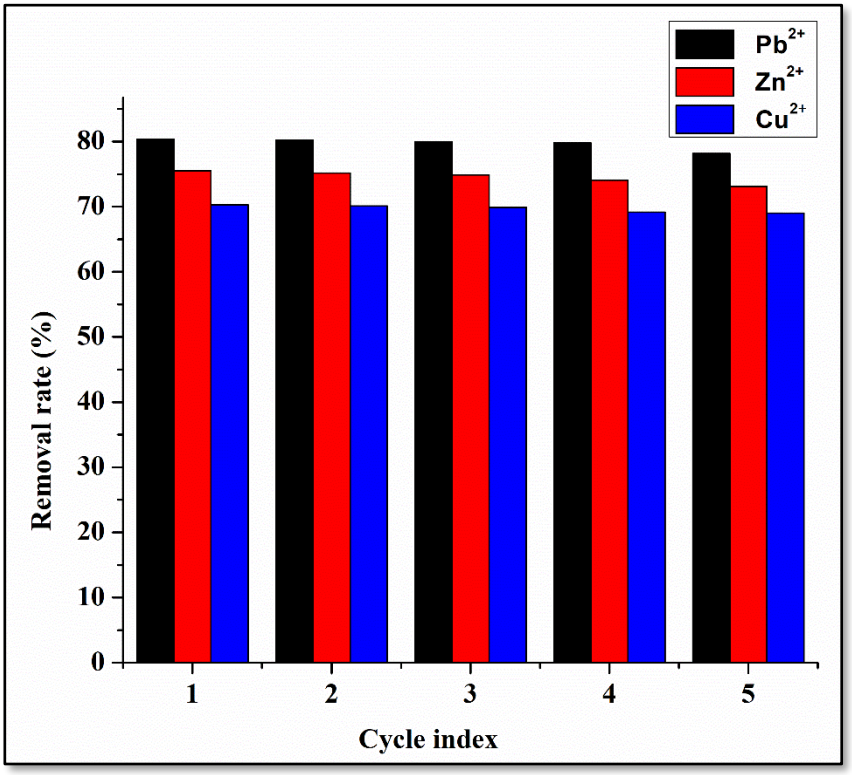

Figure 5.17. Removal rate for Pb(II), Zn(II), and Cu(II) ions throughout five consecutive cycles of reuse by polymer nanocomposite.

5.4.1. Conclusion

After conducting an elaborative study, it can be concluded that the modified biochar particles synthesized from kraft lignin, followed by modification with epichlorohydrin and triethylamine, served as an efficient, environmentally friendly, and economically viable adsorbent material. The authenticity of the synthesized modified biochar material was confirmed through various techniques, including FTIR, XPS, XRD, etc. In turn, it was utilized as a reinforcing agent along with bentonite nanoclay particles to conduct the fabrication of a nanohybrid material. The polymer nanocomposite material was further authenticated using various methods inclusive of FTIR, XPS, XRD, etc. and it exhibited enhanced mechanical as well as thermal properties as compared to other polymer nanocomposites bearing bentonite nanoclay and modified biochar particles as the

reinforcing agents. It also demonstrated excellent biodegradability attributes, and was effectively employed as adsorbents for carrying out removal of heavy metal ions, viz., Pb(II), Zn(II), and Cu(II) ions from aqueous systems, showcasing excellent removal capacity. Additionally, through elaborate kinetic analysis, the PSO kinetic model emerged as the most suitable for describing the removal of heavy metal ions, viz., Pb(II), Zn(II), and Cu(II) ions, by the polymeric nanocomposite material. Moreover, the Langmuir adsorption isotherm was found to be the most appropriate model for characterizing the sorption behavior of the polymer nanocomposite material. Overall, the polymer nanocomposite material displayed outstanding sustainability, accompanied by economic feasibility and satisfactory recovery capabilities.

References

[1] Demarchi, C. A., Michel, B. S., Nedelko, N., Ślawska-Waniewska, A., Dłużewski, P., Kaleta, A., Minikayev, R., Strachowski, T., Lipińska, L., Dal Magro, J., and Rodrigues, C. A. Preparation, characterization, and application of magnetic activated carbon from termite feces for the adsorption of Cr (VI) from aqueous solutions. *Powder Technology*, 354:432-441, 2019.

[2] Shan, Y., Yang, W., Li, Y., Liu, Y., and Pan, J. Preparation of microwave-activated magnetic bio-char adsorbent and study on removal of elemental mercury from flue gas. *Science of the Total Environment*, 697:134049, 2019.

[3] Maneechakr, P. and Karnjanakom, S. Environmental surface chemistries and adsorption behaviors of metal cations (Fe^{3+}, Fe^{2+}, Ca^{2+} and Zn^{2+}) on manganese dioxide-modified green biochar. *RSC Advances*, 9(42):24074-24086, 2019.

[4] Choi, H. D., Jung, W. S., Cho, J. M., Ryu, B. G., Yang, J. S., and Baek, K. Adsorption of Cr (VI) onto cationic surfactant-modified activated carbon. *Journal of Hazardous Materials*, 166:642-646, 2009.

[5] Cui, J., Jing, C., Che, D., Zhang, J., and Duan, S. Groundwater arsenic removal by coagulation using ferric (III) sulfate and polyferric sulfate: a comparative and mechanistic study. *Journal of Environmental Sciences*, 32:42-53, 2015.

[6] Liu, W., Zhang, J., Zhang, C., Wang, Y., and Li, Y. Adsorptive removal of Cr (VI) by Fe-modified activated carbon prepared from Trapa natans husk. *Chemical Engineering Journal*, 162(2):677-684, 2010.

[7] Nejadshafiee, V., and Islami, M. R. Adsorption capacity of heavy metal ions using sultone-modified magnetic activated carbon as a bio-adsorbent. *Materials Science and Engineering: C*, 101:42-52, 2019.

[8] Feng, N. C., Wei, F. A. N., Zhu, M. L., and Guo, X. Y. Adsorption of Cd^{2+} in aqueous solutions using $KMnO_4$-modified activated carbon derived from Astragalus residue. *Transactions of Nonferrous Metals Society of China*, 28(4):794-801, 2018.

[9] Fidel, R. B., Laird, D. A., and Thompson, M. L. Evaluation of modified Boehm titration methods for use with biochars. *Journal of Environmental Quality*, 42(6):1771-1778, 2013.

[10] Li, X., Cao, Y., Xiao, J., Salam, M. M. A., and Chen, G. Bamboo biochar greater enhanced Cd/Zn accumulation in Salix psammophila under non-flooded soil compared with flooded. *Biochar*, 4(1):7, 2022.

[11] Wang, L., Bolan, N. S., Tsang, D. C., and Hou, D. Green immobilization of toxic metals using alkaline enhanced rice husk biochar: Effects of pyrolysis temperature and KOH concentration. *Science of the Total Environment*, 720:137584, 2020.

[12] Zhao, Y., Zhang, R., Liu, H., Li, M., Chen, T., Chen, D., Zou, X., and Frost, R. L. Green preparation of magnetic biochar for the effective accumulation of Pb (II): Performance and mechanism. *Chemical Engineering Journal*, 375:122011, 2019.

[13] Shen, W., Li, Z., and Liu, Y. Surface chemical functional groups modification of porous carbon. *Recent Patents on Chemical Engineering*, 1(1):27-40, 2008.

[14] Sun, C., Chen, T., Huang, Q., Wang, J., Lu, S., and Yan, J. Enhanced adsorption for Pb (II) and Cd (II) of magnetic rice husk biochar by $KMnO_4$ modification. *Environmental Science and Pollution Research*, 26:8902-8913, 2019.

[15] Xiang, J., Lin, Q., Cheng, S., Guo, J., Yao, X., Liu, Q., Yin, G., and Liu, D. Enhanced adsorption of Cd (II) from aqueous solution by a magnesium oxide–rice husk biochar composite. *Environmental Science and Pollution Research*, 25:14032-14042, 2018.

[16] Zhou, L., Huang, Y., Qiu, W., Sun, Z., Liu, Z., and Song, Z., 2017. Adsorption properties of nano-MnO_2–biochar composites for copper in aqueous solution. *Molecules*, 22(1):173, 2017.

[17] Kar, A., Rather, M. A., Mandal, M., and Karak, N. Elastomeric biodegradable poly (ester amide urethane) as a tough and robust material. *Progress in Organic Coatings*, 182:107684, 2023.

[18] Dashamiri, S., Ghaedi, M., Dashtian, K., Rahimi, M. R., Goudarzi, A., and Jannesar, R. Ultrasonic enhancement of the simultaneous removal of quaternary toxic organic dyes by CuO nanoparticles loaded on activated carbon: central composite design, kinetic and isotherm study. *Ultrasonics Sonochemistry*, 31:546-557, 2016.

[19] Chang, J., Ma, J., Ma, Q., Zhang, D., Qiao, N., Hu, M., and Ma, H. Adsorption of methylene blue onto Fe_3O_4/activated montmorillonite nanocomposite. *Applied Clay Science*, 119:132-140, 2016.

[20] Karunanayake, A. G., Todd, O. A., Crowley, M., Ricchetti, L., Pittman Jr, C. U., Anderson, R., Mohan, D., and Mlsna, T. Lead and cadmium remediation using magnetized and non-magnetized biochar from Douglas fir. *Chemical Engineering Journal*, 331:480-491, 2018.

[21] Raju, G. M., Dakshayini, B. S., Madhu, G. M., Khan, M. A., and Reddy, P. D. S. Characterizing and modeling of mechanical properties of epoxy polymer composites reinforced with bentonite clay. *Materials Today: Proceedings*, 5(14):28098-28107, 2018.

[22] Peiris, C., Nayanathara, O., Navarathna, C. M., Jayawardhana, Y., Nawalage, S., Burk, G., Karunanayake, A. G., Madduri, S. B., Vithanage, M., Kaumal, M. N., and Mlsna, T. E. The influence of three acid modifications on the physicochemical characteristics of tea-waste biochar pyrolyzed at different temperatures: a comparative study. *RSC Advances*, 9(31):17612-17622, 2019.

[23] Zhao, S. X., Ta, N., and Wang, X. D. Effect of temperature on the structural and physicochemical properties of biochar with apple tree branches as feedstock material. *Energies*, 10(9):1293, 2017.

[24] Inyang, M., Gao, B., Yao, Y., Xue, Y., Zimmerman, A. R., Pullammanappallil, P., and Cao, X. Removal of heavy metals from aqueous solution by biochar derived from anaerobically digested biomass. *Bioresource Technology*, 110:50-56, 2012.

[25] Arash, B., Wang, Q., and Varadan, V. K. Mechanical properties of carbon nanotube/polymer composites. *Scientific Reports*, 4(1):6479, 2014.

[26] Bocchio, J., Ross, P., Sevilla, G., and Quagliano, J. Mechanical and Thermal Properties of Polyurethane Nanocomposites: Influence of Bentonite Nanoclay. *Advanced Science, Engineering and Medicine*, 9(1):53-57, 2017.

[27] Ge, F., Li, M. M., Ye, H., and Zhao, B. X. Effective removal of heavy metal ions Cd^{2+}, Zn^{2+}, Pb^{2+}, Cu^{2+} from aqueous solution by polymer-modified magnetic nanoparticles. *Journal of Hazardous Materials*, 211:366-372, 2012.

[28] Bagbi, Y., Sarswat, A., Mohan, D., Pandey, A., and Solanki, P. R. Lead (Pb^{2+}) adsorption by monodispersed magnetite nanoparticles: Surface analysis and effects of solution chemistry. *Journal of Environmental Chemical Engineering*, 4(4):4237-4247, 2016.

[29] Edathil, A. A., Shittu, I., Zain, J. H., Banat, F., and Haija, M. A. Novel magnetic coffee waste nanocomposite as effective bioadsorbent for Pb (II) removal from aqueous solutions. *Journal of Environmental Chemical Engineering*, 6(2):2390-2400, 2018.

[30] Alvarez, N. M. M., Pastrana, J. M., Lagos, Y., and Lozada, J. J. Evaluation of mercury (Hg^{2+}) adsorption capacity using exhausted coffee waste. *Sustainable Chemistry and Pharmacy*, 10:60-70, 2018.